KINEMATIC ORBIT DETERMINATION OF LOW EARTH ORBIT SATELLITES USING GPS AND GALILEO OBSERVATIONS

A THESIS SUBMITTED TO
THE GRADUATE SCHOOL OF NATURAL AND APPLIED SCIENCES
OF
MIDDLE EAST TECHNICAL UNIVERSITY

BY

OZAN KILIÇ

IN PARTIAL FULFILLMENT OF THE REQUIREMENTS
FOR
THE DEGREE OF MASTER OF SCIENCE
IN
GEODETIC AND GEOGRAPHIC INFORMATION TECHNOLOGIES

JULY 2019

Approval of the thesis:

KINEMATIC ORBIT DETERMINATION OF LOW EARTH ORBIT SATELLITES USING GPS AND GALILEO OBSERVATIONS

submitted by **OZAN KILIÇ** in partial fulfillment of the requirements for the degree of **Master of Science in Geodetic and Geographic Information Technologies Department, Middle East Technical University** by,

Prof. Dr. Halil Kalıpçılar
Dean, Graduate School of **Natural and Applied Sciences** ________________

Prof. Dr. Zuhal Akyürek
Head of Department, **Geodetic and Geographic Inf. Tech.** ________________

Prof. Dr. Mahmut Onur Karslıoğlu
Supervisor, **Geodetic and Geographic Inf. Tech., METU** ________________

Examining Committee Members:

Prof. Dr. Zuhal Akyürek
Civil Engineering, METU ________________

Prof. Dr. Mahmut Onur Karslıoğlu
Geodetic and Geographic Information Technologies, METU ________________

Prof. Dr. Haluk Özener
KOERI, Bogazici University ________________

Assoc. Prof. Dr. Uğur Murat Leloğlu
Geodetic and Geographic Information Technologies, METU ________________

Assist. Prof. Dr. Kamil Teke
Geomatics Engineering, Hacettepe University ________________

Date:

I hereby declare that all information in this document has been obtained and presented in accordance with academic rules and ethical conduct. I also declare that, as required by these rules and conduct, I have fully cited and referenced all material and results that are not original to this work.

Name, Surname: Ozan Kılıç

Signature :

ABSTRACT

KINEMATIC ORBIT DETERMINATION OF LOW EARTH ORBIT SATELLITES USING GPS AND GALILEO OBSERVATIONS

Kılıç, Ozan
M.S., Department of Geodetic and Geographic Information Technologies
Supervisor: Prof. Dr. Mahmut Onur Karslıoğlu

July 2019, 87 pages

The GNSS code measurements are used to calculate the orbits of low earth orbiting satellites. Kinematic orbit determination is an approach which is based on satellite to satellite tracking of the GNSS receivers that are mounted onboard the satellites. This approach of orbit determination is independent of satellite dynamics (e.g. gravity field, air-drag etc.) and orbit characteristics (e.g. orbit height, eccentricity etc.) and kinematic precise orbit determination can be subsequently used in gravity field estimation procedures. Inclusion of Galileo measurements besides GPS observations can increase the reliability, robustness and accuracy of real-time navigation system of the spacecraft. The major aim of this thesis is to determine the orbit of a Low Earth Orbit (LEO) satellite with Kinematic Orbit Determination approach using GPS and Galileo observations. However, the observations from Galileo constellation are not fully available, since the system has not reached Full Operational Capability (FOC) yet. Hence, the corresponding observations are simulated. Real GPS data and simulated Galileo observations are used in a Kalman Filter to estimate the position and the velocity of a LEO satellite. An Adaptive Robust Extended Kalman

Filter algorithm which is an extension of Kalman filter for non-linear systems is used particularly to enhance the filter performance in terms of accuracy. To obtain precise orbit of the satellite, the ionospheric effects are removed by taking ionosphere free linear combination of the dual-frequency GNSS measurements. Additionally, a Helmert variance component estimation (HVCE) is adopted for the estimation of variance components of each GNSS sensor measurement. In order to determine the accuracy of the estimated orbit, the results of Adaptive Robust Extended Kalman Filter algorithm for real LEO satellite data are compared with publicly available very precise ephemerides from Jet Propulsion Laboratory (JPL). Filter results from simulated navigation data are also compared with the true orbit generated by the simulation. Adaptive Robust Extended Kalman Filter algorithm is shown to provide an improvement of more than 70 cm in 3D RMS results for 24 hours of navigation data. In the simulation scenario, addition of simulated Galileo observations and implementation of HVCE approach led to achieve 20 cm better 3D RMS results.

Keywords: GNSS, Galileo, kinematic orbit determination, Kalman filter, adaptive, robust, variance component estimation

ÖZ

GPS VE GALILEO GÖZLEMLERİ KULLANILARAK YERE YAKIN UYDULARIN KİNEMATİK YÖRÜNGELERİNİN BELİRLENMESİ

Kılıç, Ozan
Yüksek Lisans, Jeodezi ve Coğrafi Bilgi Teknolojileri Bölümü
Tez Yöneticisi: Prof. Dr. Mahmut Onur Karslıoğlu

Temmuz 2019 , 87 sayfa

Yere yakın uyduların yörüngelerinin hesaplanmasında GNSS kod ölçüleri kullanılmaktadır. Kinematik yörünge tespiti, yere yakın uyduların üzerine yerleştirilmiş GNSS alıcılarının uydudan uyduya izleme yöntemine dayalı bir yaklaşımdır. Yörünge tespitinde kullanılan bu yaklaşım, uydu dinamikleri ve yörünge karakteristiklerinden bağımsızdır ve kinematik hassas yörünge tespiti gravite alanı kestirimlerinde kullanılmaktadır. Yörünge tespitinde GPS gözlemlerine ek olarak Galileo sistemine ait ölçülerin kullanılması uzay aracının gerçek-zamanlı navigasyon sisteminin güvenilirliğini, sağlamlığını ve doğruluğunu arttırabilir. Bu tezin ana hedefi yere yakın uyduların yörüngelerini, GPS ve Galileo gözlemleri kullanılarak kinematik yörünge tespiti yaklaşımı ile belirlemektir. Fakat sistem henüz Tam Operasyonel Yetenek (FOC) durumunda olmadığı için Galileo konumlama sisteminin gözlemleri tamamıyla kullanılabilir değildir. Bu sebeple, bu gözlemlerin simülasyonu gerçekleştirilmiştir. GPS verileri ve simüle edilmiş Galileo gözlemleri, alçak yörünge uydusunun konumunu ve hızını kestirmek için Kalman Filtresinde kullanılmıştır. Filtre performansını geliştirmek için doğrusal olmayan sistemlerde kullanılan bir uzantı olan, Adaptif Gürbüz Genişletilmiş Kalman Filtresi kullanılmıştır. Alçak yörünge uydusunun yörüngesini hassas olarak elde etmek için iyonosferik etkiler, çift-frekanslı GNSS ölçümlerinin doğrusal frekans kombinasyonu kullanılarak elimine edilmiştir. Ayrıca, farklı GNSS sensör ölçülerininin varyans bileşenlerinin kestirimi için Helmert Varyans Bileşeni Kestirimi (HVCE) uygulanmıştır. Hesaplanan yörüngenin doğruluğunu belirlemek amacıyla Adaptif Gürbüz Genişletilmiş Kalman filtreleme algoritmasının sonucunda bir alçak yörünge uydusuna ait gerçek verilerden elde edilen kestirilmiş yörünge verileri, Jet Propulsion Laboratory (JPL) tarafından sunulan yüksek hassasiyetli efemeris verileri ile karşılaştırılmıştır. Simüle edilmiş verilerden elde edilen filtre sonuçları, simülasyondan üretilmiş gerçek yörünge verileri ile karşılaştırılmıştır. Adaptif Gürbüz Genişletilmiş Kalman filtreleme algoritması, 24 saatlik navigasyon verisi için üç boyutlu karesel ortalama hata sonuçlarında 70 cm iyileştirme sağlamıştır. Simülasyon sonucunda elde edilmiş Galileo gözlemlerinin veri setine eklenmesi ve HVCE yönteminin uygulanması sonucunda ise üç boyutlu karesel ortalama hata sonuçları 20 cm geliştirilmiştir.

Anahtar Kelimeler: GNSS, Galileo, kinematik yörünge tespiti, Kalman filtresi, adaptif, robust, varyans bileşen kestirimi

To my family

ACKNOWLEDGMENTS

I would like to thank my supervisor Prof. Dr. Mahmut Onur Karslıoğlu for his continuous support and guidance throughout my thesis study. His immense knowledge, encouragement, critical comments and suggestions motivated me to complete this study.

Besides, I would like to express my appreciation to examining committee members Prof. Dr. Zuhal Akyürek, Assoc. Prof. Dr. Uğur Murat Leloğlu, Prof. Dr. Haluk Özener and Assist. Prof. Dr. Kamil Teke for their valuable suggestions, comments and critics.

Furthermore, I am also grateful to my colleagues Raşit Uluğ, Feyza Sakil and Eyüp Sopacı for their endless support and motivation. Specially, I would like to thank Amir Yeganehsahab for his unique support and continuous encouragement in every step of this process.

Finally, I must express my very profound gratitude to my parents and my sister for their constant love and support throughout this process. It would be impossible for me to do this study without them.

TABLE OF CONTENTS

CHAPTERS

LIST OF TABLES

TABLES

LIST OF FIGURES

FIGURES

LIST OF ABBREVIATIONS

3D	3 Dimensional
AREKF	Adaptive Robust Extended Kalman Filter
CDDIS	The Crustal Dynamics Data Information System
CEKF	Classical Extended Kalman Filter
CHAMP	Challenging Minisatellite Payload
ECEF	Earth-centered Earth-fixed
ECI	Earth-centered Inertial
EKF	Extended Kalman Filter
GEO	Geostationary Earth Orbit
GNSS	Global Navigation and Satellite System
GPS	Global Positioning System
GLONASS	GLObal NAvigation Satellite System
GOCE	Gravity field and Ocean Circulation Explorer
GRACE	The Gravity Recovery and Climate Experiment
HEO	High Earth Orbit
HVCE	Helmert Variance Component Estimation
IERS	International Earth Rotation and Reference Systems Service
IGS	International GNSS Service
JPL	Jet Propulsion Laboratory
LEO	Low Earth Orbit
MEO	Medium Earth Orbit
MGEX	The Multi-GNSS Experiment
OD	Orbit Determination
POD	Precise Orbit Determination

RINEX	Receiver Independent Exchange Format
RMS	Root Mean Square
RK4	Runge-Kutta 4th Order
SLR	Satellite Laser Ranging
SAR	Synthetic Aperture Radar
TDRS	Tracking and Data Relay Satellite
TRSR	Turbo Rogue Space Receiver

CHAPTER 1

INTRODUCTION

1.1 Research Background

Over the past decades, a large number of Low Earth Orbit (LEO) satellites have been launched for scientific and commercial purposes into the orbits at the altitudes from 300 km to 2000 km. As these satellites carry advanced high resolution sensors such as gradiometer, digital cameras or radar, there is a need for precise, accurate and reliable position information for high quality products. Orbit determination has been applied for various of applications such as spacecraft trajectory analysis, geolocation of remote sensing observations, gravity field determination, sea surface topography, radar altimetry and synthetic aperture radar based imaging.

The main objective of orbit determination is to obtain accurate state information along the orbital path in a dynamical environment which includes relevant forces affecting orbital motion of the satellite (Vetter, 2007). There are various external forces that influence satellite's motion. Gravity of the Earth, atmospheric drag, solar radiation pressure, third-body perturbations as a direct effect of gravity of sun, moon and the other planets, Earth and ocean tidal effects, and general relativity can be considered as the main forces constituting the nonlinear equation of motion of the satellite. Orbit determination comprises the solution of these equations with different techniques. Kinematic orbit determination is a special kind of orbit determination method, which allows state estimation independently of these forces acting on the satellite. On the contrary to the common reduced-dynamic approach, kinematic orbit determination is highly dependent on the observations which affect the accuracy directly. For this reason, it can be considered as an observation driven approach.

Orbit determination of LEO satellites requires accurate position and velocity information. In recent years, satellite tracking systems which measure directly the distance between the transmitter and the receiver are used to obtain these measurements (Jäggi and Arnold, 2017). Global Positioning System (GPS) receivers onboard the satellites are preferred as the primary tracking system due to their global coverage, continuous tracking capability, and accurate positioning performance for orbit determination of LEO satellites (Karslioglu et al., 2017). Accurate estimation of satellite state parameters in real-time or off-line with post processing is possible with GPS sensor mounted on the satellite. Using dual-frequency observations and ground-based orbit determination algorithms, it is possible to obtain sub-meter level accuracy for the satellites in LEO (Montenbruck et al., 2008). GPS-based orbit determination is used in several scientific space missions such as GRACE, GOCE, CHAMP and TOPEX/Poseidon and proved itself as a low cost, accurate and reliable technique for orbit determination. These missions have benefited from on-board spaceborne GPS receivers, and the measurements obtained from GPS satellites are used as observations for orbit determination.

Besides GPS positioning, other satellite navigation systems with global coverage such as GLONASS, Galileo and BeiDou started to provide satellite-based positioning. Newly developed ground-based receivers are developed to be compatible with the signals of other navigation systems. Since European navigation system Galileo, offers a promising signal plan, its contribution to Global Navigation Satellite System (GNSS) are studied in Basile et al. (2018). Using the multi-GNSS measurements is considered to be more reliable and highly accurate in terms of position estimation (Biswas et al., 2014). According to Fu et al. (2019) using combination of GPS and Galileo observations improves positioning accuracy by almost 50 percent.

One of the most important contributions of multi-GNSS positioning is its effect in Dilution of Precision (DOP). As the variety of GNSS satellite distribution increases, DOP values are expected to be better. Consequently, the number of satellites is significantly important for satellite positioning. In Capuano et al. (2013) both GPS and Galileo constellation are analyzed in terms of geometrical availability and signal power for MEO, GEO and HEO. Thus far, there is no accuracy information obtained regarding to Galileo observations. Nonetheless, some simulations are performed

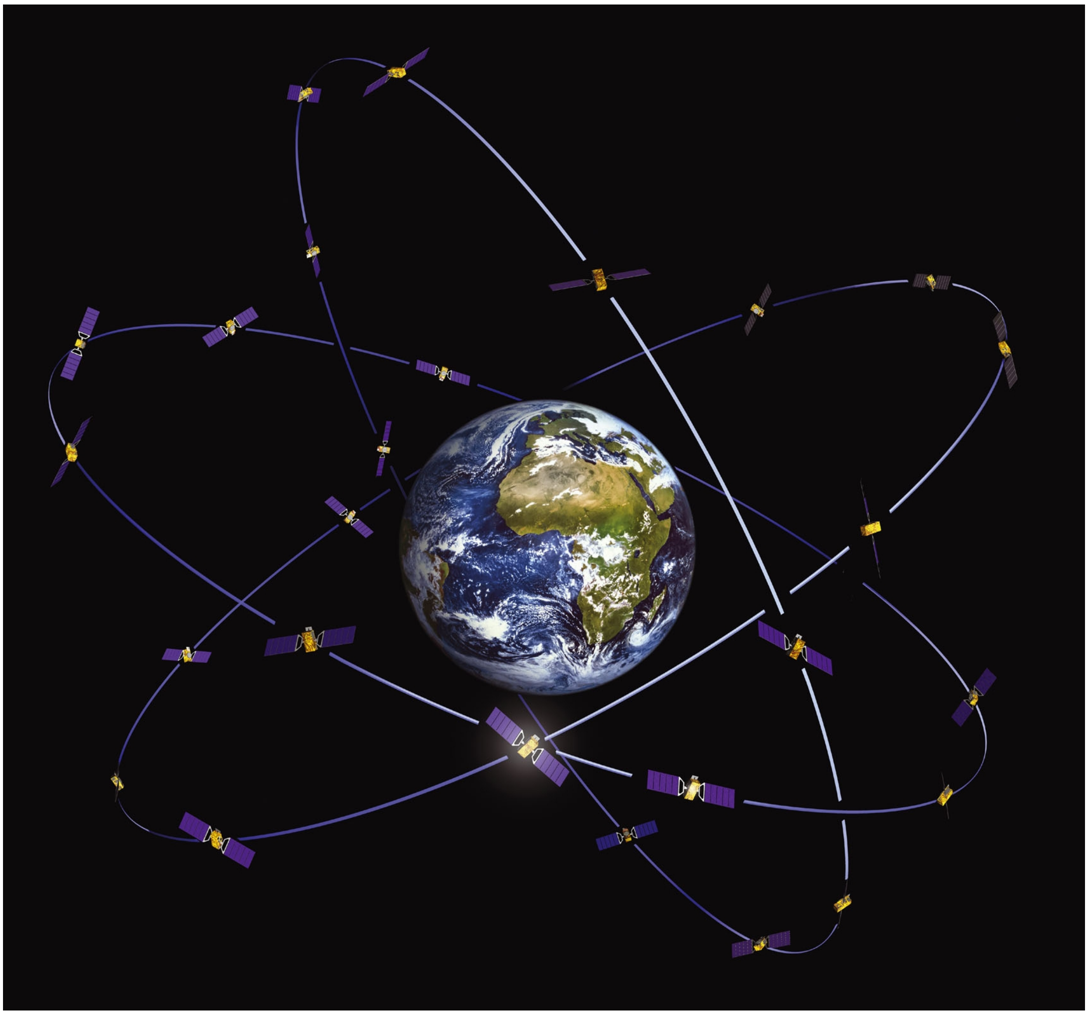

Figure 1.1: Planned Galileo Constellation *Credit: ESA*

to generate raw GNSS data to process. Biswas et al. (2014) used hardware-based GNSS simulator to generate measurements and proved Galileo's contribution in a general manner. However, the RMS results for using real navigation data were significantly large due to simple orbit, clock modeling and reference interval used in orbit propagation.

1.2 Motivation and Objective

GNSS-based orbit determination is widely used technique for the determination of LEO satellite orbits. Due to its low-cost and easily applicable structure, it is preferred among all orbit determination techniques for recent space missions. General information about these techniques and satellite orbits is given in Chapter 2. GNSS positioning and its use in orbit determination, GNSS measurements and different orbit determination algorithms are explained in Chapter 3.

The goal of this thesis is to estimate the satellite state vectors by using both GPS and Galileo measurements. Since Galileo measurements are not completely available, a software-defined GNSS satellite simulator is developed to generate raw Galileo measurements. GNSS satellite simulation is detailed in Chapter 4. In order to process the data generated from the simulator, a particular extension of Kalman filter is used to perform accurate state estimation. Kalman filters are preferred commonly in orbit determination due to their low computational cost and real-time compatible structure. An Extended Kalman filter for nonlinear systems is modified in terms of adaptivity and robustness. Adaptive Robust Extended Kalman filter is proposed by Yang (2010) to deal with measurement outliers and system uncertainties. Since measurements are vitally important for kinematic orbit determination, using an adaptive robust estimation is expected to improve the filter performance. Adaptive robust estimation is detailed in Chapter 5.

Additionally, Gao et al. (2016) proposed a Helmert Variance Component based Adaptive Kalman Filter algorithm to be used in multi-GNSS applications. Variance component estimation is known with weighting the observations from different sensors, and it should be used with measurements with no outliers. Outlier detection and removal procedure should be performed beforehand. However, it has not been used with a robust filter which also deals with outliers. In this thesis, Variance component estimation algorithm is integrated into a robust filter with the help of a robust scale factor (see Chapter 5). Chapter 6 comprises the results of AREKF approach and HVCE implementation. The results are discussed in the Chapter 6 and concluded with a summary in Chapter 7.

CHAPTER 2

ORBIT DETERMINATION

2.1 Satellite Orbits

A satellite orbit is the path of a satellite which is moving around another celestial body under the main influence of gravitation. According to Newton's law of gravitation, gravity keeps all satellites in near circular or elliptical motion around the earth. Satellite orbits around the earth can be defined particularly according to their synchronicity, inclination, eccentricity, and altitude. The majority of the satellites and the space stations take place in Low Earth Orbit (LEO) due to its accessibility in terms of servicing and communication. Therefore, orbit determination of LEO satellites has significant importance for space navigation.

A satellite state can be expressed in two forms. In both forms, six parameters are needed. These parameters can be a set of elements called *orbital elements* which are the scalar magnitudes and angular representations of the orbit and its orbital plane. On the other hand, the satellite state can be defined with the *state vector* consists of three components of position and velocity vectors. In this thesis, state representation will be in state vector form with a few additional parameters.

2.2 Orbital Perturbations and Orbit Modeling

Satellite orbit modeling is the simulation of a satellite trajectory mathematically according to its orbital motion around the Earth under gravitational and non-gravitational forces. Modeling all these related forces is also called as *force modeling*. The Keplerian orbit considers only the gravitational attraction of two celestial bodies. Therefore, the deviations from this orbit are commonly called as *perturbation*. The perturbations due to various geopotential coefficients $J_{n,m}$, atmospheric drag, solar radiation pressure, tidal effects, and relativistic effects are the examples of these perturbations. The effect of these perturbations on the acceleration of different satellites (Iridium, Lageos, GPS and TDRS) can be seen in Figure 2.1. In this thesis, orbital perturbations are not explained in detail, since only pure geometry is needed for kinematic orbit determination which will be defined in Section 3.2.3.

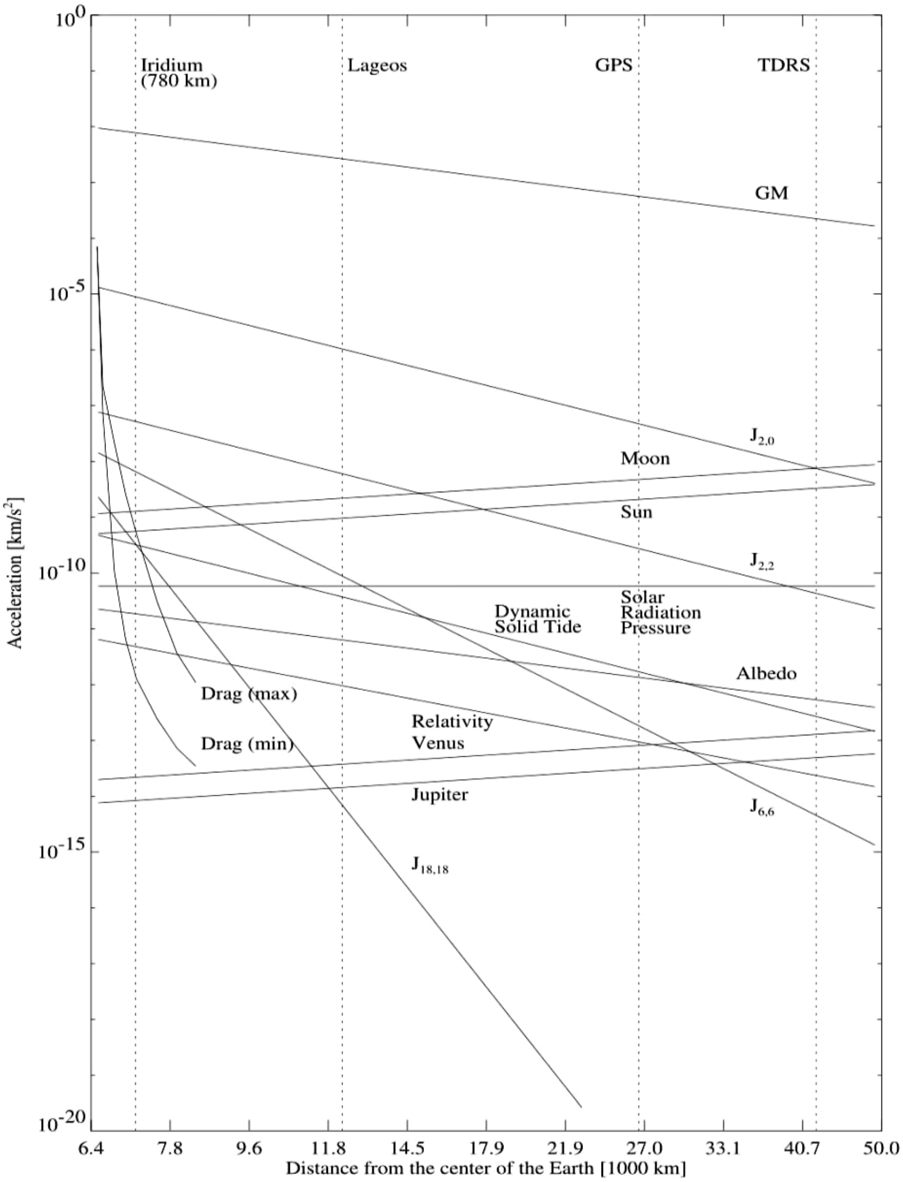

Figure 2.1: Order of magnitude of various perturbations of a satellite orbit (Montenbruck and Gill, 2012)

2.3 Orbit Propagation and Numerical Integration

Satellite orbit propagation is the transmission of the orbital motion of the satellite at a time and direction using an initial position and velocity information. During orbit propagation, a prediction procedure is performed at each time step. To obtain high accuracy orbits, numerical methods are required for the solution of the equation of motion.

In celestial mechanics, numerical methods are widely used to solve differential equations. Various numerical methods such as Runge-Kutta, multistep and extrapolation methods are developed in the past (Montenbruck, 1992). Each numerical method has particular use for the prediction of the satellite motion. Runge-Kutta is a stable and common method which is used in many applications. Since an accurate prediction is not needed in kinematic orbit determination, Runge-Kutta method can be used for numerical integration of the equation of the orbital motion according to Newton's law of gravitation. Owing to its simplicity, the 4th-order Runge-Kutta (RK4) method is preferred in this thesis. More information about other numerical integration methods can be found in Montenbruck and Gill (2012); Butcher (2016).

2.4 Fourth Order Runge-Kutta Method

For satellite orbit propagation, the 4th order Runge-Kutta method can be used for a modest estimate. For a state vector $\vec{x}$ with position $\vec{r}$ and velocity $\vec{v}$ components derivative of the state with respect to time t can be expressed with a function f:

$$f(t,x) = \frac{\partial \mathbf{x}}{\partial t} = \begin{pmatrix} \dot{\mathbf{r}} \\ \ddot{\mathbf{r}} \end{pmatrix} \tag{2.1}$$

where the dots denote the order of the derivative with respect to the time. The first and the second derivative of the position are given as:

$$\dot{\mathbf{r}} = \mathbf{v} \tag{2.2}$$

and

$$\ddot{\mathbf{r}} = -\frac{GM_E}{r^3}\mathbf{r} \tag{2.3}$$

where G is the Earth's gravitational constant and M_E is the Earth's mass which can be taken as $6.67408 \times 10^{-11}\ m^3kg^{-1}s^{-2}$ and $5.972 \times 10^{24}\ kg$, respectively. The approximation of x for the next step is possible with a simple *Euler step* as follows:

$$x_{(t_0+h)} = x_0 + f(t_0, x_0) \cdot h \tag{2.4}$$

where h is the step size time and x_0 is the initial value of x. The equation can be rewritten with an increment function as:

$$x_{(t_0+h)} \approx x_0 + \phi \cdot h \tag{2.5}$$

where ϕ is the weighted average of the slope approximation. Expansion of Taylor series up to 4th order is given as:

$$x_0 + \dot{x}_0 h + \frac{h^2}{2!}y_0^2 + \frac{h^3}{3!}y_0^3 + \frac{h^4}{4!}y_0^4 \tag{2.6}$$

Since Taylor's method requires function differentiation for each order, Runge-Kutta methods provide a numerical solution with evaluating the original function f, only. Weighted average of the 4th order slope approximation can be calculated as:

$$\phi = \frac{1}{6}(k_1 + 2k_2 + 2k_3 + k_4) \tag{2.7}$$

where k_1, k_2, k_3, k_4 are the slope approximations which can be given as:

$$\begin{aligned} k_1 &= f(t_0, x_0) \\ k_2 &= f(t_0 + \frac{h}{2}, x_0 + \frac{hk_1}{2}) \\ k_3 &= f(t_0 + \frac{h}{2}, x_0 + \frac{hk_2}{2}) \\ k_4 &= f(t_0 + h, x_0 + hk_3) \end{aligned} \tag{2.8}$$

The 4th order Runge-Kutta method is very well suited in terms of the complexity and storage requirements since low-order Runge-Kutta methods are widely preferred in onboard applications, as they are relatively fast, accurate and stable at large time steps (Tukaram, 2014).

2.5 Orbit Determination Techniques

As it is mentioned in Section 2.1, determination of satellite orbits has a crucial role in LEO spacecraft missions. As the number of missions increase, the feasibility of orbit determination becomes more important. There are various orbit determination techniques performed depending on the mission requirements and objectives. These techniques can be grouped under two main headings as ground-based and space-based orbit determination techniques which are explained in the following sections.

2.5.1 Ground-Based Orbit Determination

Various ground-based techniques are developed in the past to determine satellite orbits. Radar, laser and optical measurements are used to determine the position of the satellite simply by measuring range and angle. Among these approaches, Satellite Laser Ranging (SLR) is the most accurate technique with sub-cm level accuracy. SLR is often used for validation of satellite orbits which are determined by other techniques. The distance between satellite and ground station is calculated basically by measuring the travel time of a laser pulse which is transmitted from the station and reflected back to the station by the retroreflectors on the satellites (See Fig. 2.2).

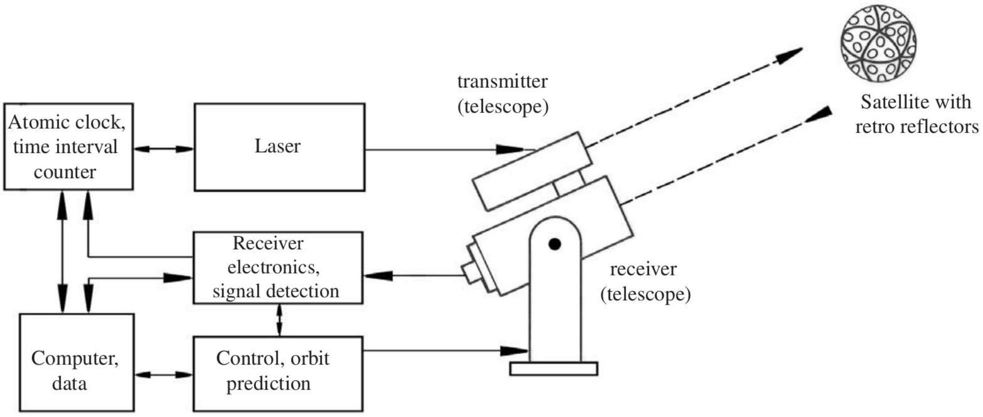

Figure 2.2: Working principle of Satellite Laser Ranging (SLR) (Seeber, 2003)

Although ground-based techniques provide direct and reliable measurements, they are not very efficient in terms of cost and time. A network of ground stations is required to be established around the world to track the satellites continuously. The homogeneity of the data distribution is dependent on the number of stations on the earth. Nevertheless, ground-based orbit determination techniques are preferred to ensure data quality and reliability (Karslioglu, 2005).

2.5.2 Space-Based Orbit Determination

Each space-based system for orbit determination is uniquely named with respect to the type of data acquisition method. Numerous techniques are presented in the past such as magnetometer-based orbit determination (Psiaki et al., 1993), image-based orbit determination (Li et al., 2017b) and GPS-based orbit determination (Yunck et al., 1985). Although, they are not as accurate as SLR technique, the results achieved by space-based techniques can reach up to cm-level accuracy (Montenbruck et al., 2005; Peng and Wu, 2009). GPS-based orbit determination is the most accurate method among space-based techniques. Due to its efficiency, GPS-based orbit determination is mostly preferred for real-time precise positioning in LEO spacecraft missions.

CHAPTER 3

GNSS-BASED ORBIT DETERMINATION

Global Navigation and Satellite System (GNSS) is one of the most common positioning technique used in ground applications as well as space-based applications. Since some of the space missions (e.g. gravity field missions) require highly accurate orbit information, GNSS positioning provides accurate solution to determine the satellite's orbit. Positioning accuracy is also crucial for determination of Earth's gravity field. Besides gravity field determination, precise orbit products are also important for synthetic aperture radar (SAR) imaging which is a widely used technique in Earth observation. GNSS-based precise orbit determination is used to deliver precise orbit products for generation of high-quality SAR images (Yoon et al., 2009). Since Global Navigation and Satellite System (GNSS) offers global coverage, continuous tracking capability and high accuracy, in various missions GNSS receivers have been used onboard LEO satellites as the primary component of tracking systems for orbit determination (Erdogan, 2011).

In GNSS-Based Orbit Determination, LEO satellite's position is determined initially or during the orbit by kinematic positioning. Kinematic positioning is essentially a parameter estimation procedure to estimate the state parameters in a particular epoch.

3.1 Reference systems used and Transformations

For the definition of satellite's orbital motion a suitable reference system needs to be defined. In order to model observations and evaluate the results, geocentric coordinate systems are generally used since the satellite motion refers to the Earth's center of mass (Seeber, 2003).

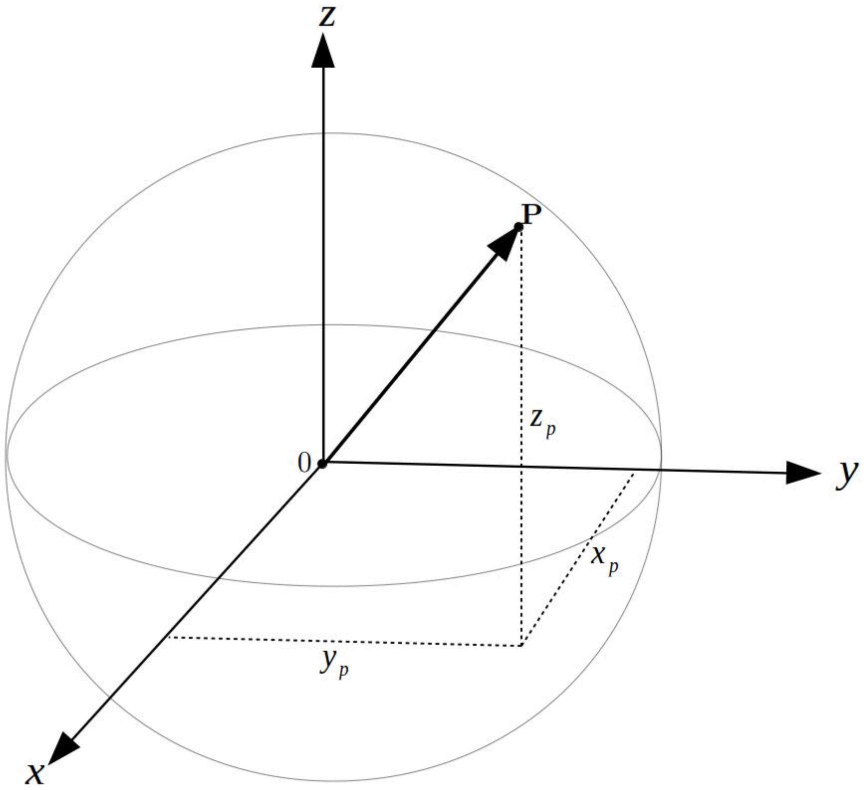

Figure 3.1: Cartesian Coordinate System

The inertial reference system is a system where it is at rest or moves uniformly without any acceleration. This system is the only system that the Newton's laws of motion are valid and is the base of the development of the theory of motion for artificial satellites.

The space fixed inertial reference systems are either tied to extra-galactic radio sources (e.g. stars and quasars) or extraterrestrial objects such as planets/Moon. Hence, they are called *celestial reference systems* (CRS). If the motion of planets, Moon or artificial satellites are taken into the consideration for the definition of a CRS, it is called *Dynamical CRS*. However if it is defined by the extra-galactic radio sources it is called *Kinematic CRS* (Seeber, 2003).

Earth-centered inertial (ECI) is commonly used coordinate system for orbit measurements and orbit determination purposes. The origin of the coordinate system is at the center of mass of the Earth and the axes point in fixed directions with respect to the stars (Kaplan and Hegarty, 2017). The orbit of a space object can be modeled in an ECI coordinate system according to the Newton's law of gravitation.

The Earth fixed reference system should be optimally connected to the earth crust. To define and realize such a Conventional Terrestrial System (CTS) a Cartesian Coordinate System (Figure 3.1) of ground stations that construct a global network can be established.

The conventional terrestrial reference system is originated at the geo-center where the mass of oceans and the atmosphere are taken into account. The Earth rotation axis is assumed to be z-axis of CTS. However because the actual origin and rotation axes of the Earth are not known, a conventional approximation for them is defined. Since 1895 the International Latitude Service (ILS) and since 1962 the International Polar Motion Service (IPMS) used astronomical observations to settle and maintain these conventions (Moritz, Mueller, 1987). The conventional Terrestrial Pole (CTP) is defined based on the mean polar axis over the period of 1900-1905, with a zero longitude on the equator (Greenwich Mean Observatory (GMO)) (Seeber, 2003).

Earth-centered Earth-fixed (ECEF) system is mainly used to determine the position of a ground object or a receiver. Using a coordinate system which rotates with the Earth is more convenient in terms of representation of the position of an object relative to the ground (Kaplan and Hegarty, 2017). The xy plane of ECEF coordinate system coincide with the Earth's equatorial plane. Transformation to geodetic latitude, geodetic longitude, and geodetic height are performed with ECEF coordinates.

Every geodetic measurement method corresponds to a specific reference coordinate system since the definition of each measurement technique differs from others. Hence, the data they obtain is different in the context of the reference coordinate systems. These methods do not necessarily use identical reference systems. The measurements that are terrestrially obtained are inherently local and described in local reference coordinate systems. To be able to handle these measurements with the observations that are obtained by other space geodetic techniques, the relationship between them has to be accurately defined. Sometimes the transformation parameters between these coordinate systems are determined with lower accuracy than the individual measurements. This can also impose an additional error to the transformed coordinates. Thus, it is very important to establish precise transformation formulas to be able to transform the observations accurately from a coordinate system to another one.

In order to obtain GNSS satellite geometry or determine the signal strength for a receiver, elevation and azimuth angles must be calculated. However, to obtain these quantities, positions need to be defined in a local coordinate system. Three-dimensional cartesian vector needs to be expressed in spatial ellipsoidal coordinates consists of geodetic latitude, longitude and height. Let ECEF cartesian position vector defined as:

$$P = \begin{bmatrix} x \\ y \\ z \end{bmatrix} \tag{3.1}$$

Longitude (λ) can be calculated from two components as:

$$\lambda = atan\left(\frac{y}{x}\right) \tag{3.2}$$

The inverse problem of φ and h can be solved by iteration. However, Bowring (1985) has given solution for geodetic latitude and height which typically converges after two or three iterations:

$$\varphi = atan\left(\frac{z + e'^2 b sin^3\theta}{\sqrt{x^2+y^2} - e^2 cos^3\theta}\right) \tag{3.3}$$

where e and e' refer to first and second numerical eccentricity, a and b refer to the length of the semi-major and the semi-minor axes and θ is given as:

$$\theta = atan\left(\frac{az}{b\sqrt{x^2+y^2}}\right) \tag{3.4}$$

And the geodetic height can be calculated as:

$$h = \frac{\sqrt{x^2 + y^2}}{cos\varphi} - N \tag{3.5}$$

where N is the radius of curvature in the vertical prime, given as:

$$N = \frac{a}{(1 - e^2 sin^2\varphi)^{1/2}} \tag{3.6}$$

The local East, North, Up (ENU) cartesian coordinate system is used in many tracking and navigation applications due to its practicality and simplicity compared to ECEF or geodetic coordinates. The local ENU coordinates are formed from a plane tangent to the Earth's surface fixed to a specific location and hence it is sometimes known as a *local tangent* or *local geodetic* plane. The unit vectors in local East, North and Up directions are expressed as:

$$\begin{aligned} \hat{\mathbf{e}} &= (-sin\lambda,\ cos\lambda,\ 0) \\ \hat{\mathbf{n}} &= (-cos\lambda sin\varphi,\ -sin\lambda sin\varphi,\ cos\varphi) \\ \hat{\mathbf{u}} &= (cos\lambda cos\varphi,\ sin\lambda cos\varphi,\ sin\varphi) \end{aligned} \tag{3.7}$$

The elevation of a geographic location is its height above or below a fixed reference point, most commonly a reference geoid, a mathematical model of the Earth's sea level as an equipotential gravitational surface. The term *elevation* is generally used when referring to a spacecraft orbiting related to a ground station or a fixed point on the Earth's surface. But it is also possible to use it for two moving objects (e.g. satellites) by defining a local coordinate system with an origin of observer's point.

The vector from an observer (origin) to a point of interest is projected perpendicularly onto a reference plane; the angle between the projected vector and a reference vector on the reference plane is called the *azimuth*.

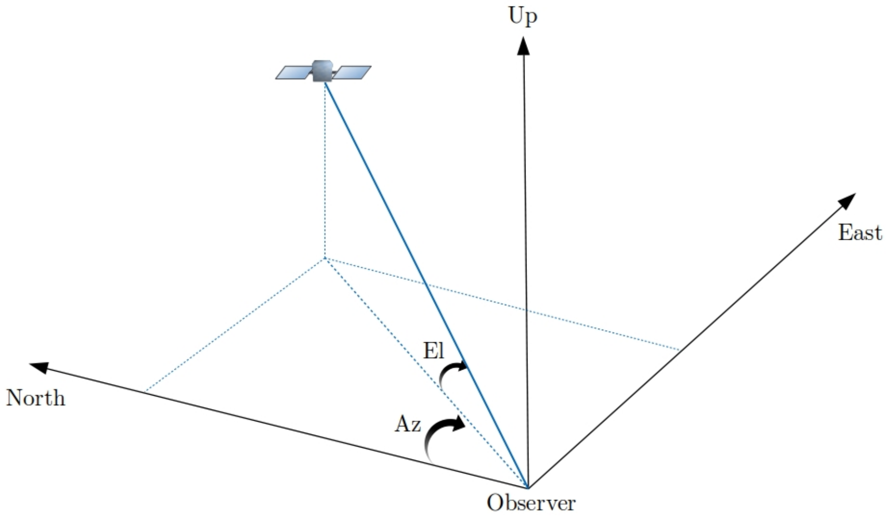

Figure 3.2: Azimuth and Elevation

The elevation and azimuth of satellite in the local coordinates system (ENU) (Figure 3.2) are computed from local unit vectors as follows:

$$A = arctan\left(\frac{\hat{\mathbf{r}} \cdot \hat{\mathbf{e}}}{\hat{\mathbf{r}} \cdot \hat{\mathbf{n}}}\right) \tag{3.8}$$

$$E = arcsin\left(\hat{\mathbf{r}} \cdot \hat{\mathbf{u}}\right) \tag{3.9}$$

where $\hat{\mathbf{r}}$ is the line of sight unit vector which can be calculated with the geocentric position of the satellite ($\mathbf{r}^{sat}$) and receiver($\mathbf{r}^{rec}$) as follows:

$$\hat{\mathbf{r}} = \frac{\mathbf{r}^{sat} - \mathbf{r}^{rec}}{||\mathbf{r}^{sat} - \mathbf{r}^{rec}||} \tag{3.10}$$

In this thesis, results are evaluated in an orbital reference system. Satellite orbital reference system which is known as RSW Reference System is generally used in orbit determination to apply relative motion of the satellite with respect to the resident space object (Zappulla and Spencer, 2013). Origin of the reference system usually coincides with the mass center of resident space object. The axes of the reference system are defined as Radial (R), Along-track (S) and Cross-track related to the position vector (**r**) from the Earth's center of mass and orbital direction. The Radial axis is simply the direction of satellite position vector extended through the satellite. The along-track (S) and the cross-track (W) axes are aligned with the orbital motion where S is generally direction of the velocity vector abd W is the direction of normal of the orbit plane. Since the orbits are not generally circular and the satellite is not at apogee or perigee in an elliptical orbit all the time, S axis does not generally coincide with the velocity vector (Erdogan, 2011). RSW reference system is illustrated in Figure 3.3.

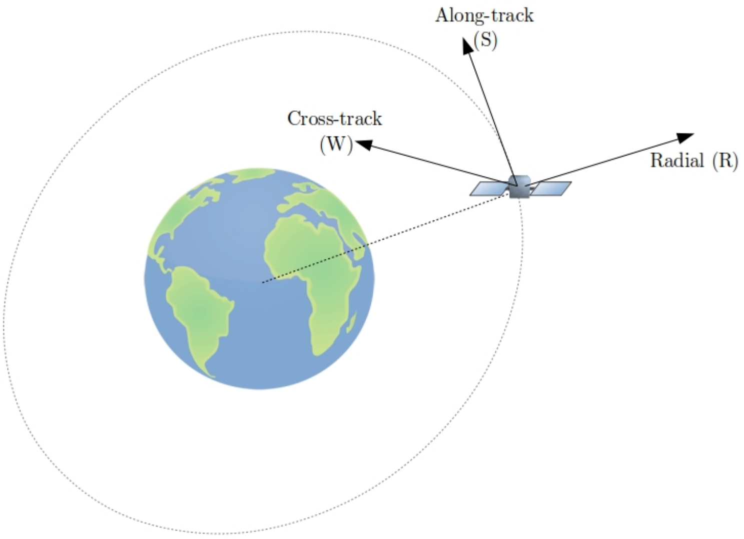

Figure 3.3: Satellite Orbital Reference System (RSW)

3.1.1 GNSS Overview

3.1.2 Observables and Measurement Modeling

In GNSS data acquisition concept, the distance between satellite and receiver is called *pseudorange* (Hofmann-Wellenhof et al., 2007). Since the quality of satellite and receiver clocks are not the same and differ from the GPS Time[1], a clock error arises for both clocks. Pseudoranges are the raw observations containing these clock errors as well as the other errors caused by different error sources such as environmental or instrumental errors. Since signal travel is directly affected by these errors, geometric distance between the satellite and the receiver are corrected with correction terms. Pseudoranges can be calculated in two ways.

3.1.2.1 Code Pseudorange

A signal transmitted from a GNSS satellite carries *pseudo-random code* to be matched with an identical code (replica) generated by the GNSS receiver. Signal travel time between the satellite and the receiver is determined by the amount of the slide until the codes are synchronized. The receiver "slides" its code continuously in time until it is synchronized with the code from satellite (See Fig. 3.4). The amount of this slide in the code is equal to the signal's travel time. Code pseudoranges are calculated by the time difference between two clocks on the satellite and the receiver. The difference between signal transmission time on the satellite t^s and the signal reception time read by the receiver t_r can be given as:

$$t_r - t^s = (t_r + \delta_r) - (t^s + \delta^s) = \Delta t + \Delta\delta \tag{3.11}$$

where δ_r and δ^s are the receiver and the satellite clock biases, respectively. By multiplying Eq. 3.11 by the speed of light, code pseudoranges can be computed as:

$$\rho = c(t_r - t^s) = c(\Delta t + \Delta\delta) \tag{3.12}$$

---

[1] A continuous time scale started by the GPS Control segment on the basis of a set of atomic clocks at the ground monitoring stations and onboard the satellites

The main problem is that the bits (or cycles) of the pseudo random codes are so wide they are not perfectly matched up. As a result code measurements are precise to the meter level.

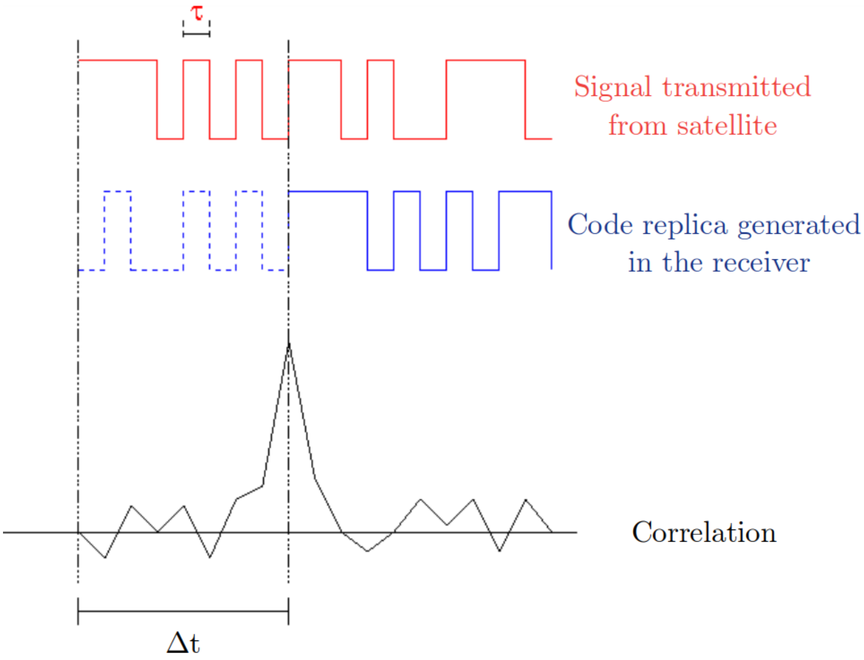

Figure 3.4: Determination of the signal traveling time by code pseudoranges

3.1.2.2 Phase Pseudorange

The carrier phase itself can be also used to measure distance between the satellite and the receiver. The noise of the carrier phase measurements are smaller when it is compared to code pseudoranges. Hence, the carrier phase measurements are more precise than the code measurements. However, they are ambiguous by an unknown integer number of wavelengths (N). This unknown number presents after the first lock on the signal and every time the receiver loses the lock on the signal due to the jumps or range discontinuities, this ambiguity changes arbitrarily. The beat phase of the phase of the received signal and receiver generated reference phase, $\varphi_s^r(t)$, can be obtained as follows:

$$\varphi_s^r(t) = \Delta\varphi_s^r(t) + N \tag{3.13}$$

where t is the time epoch with respect to initial time t_0 , N is the integer ambiguity term and $\Delta\varphi_s^r(t)$ is the fractional part of the phase. Instantaneous fractional phase can be measured after signal lock but the integer ambiguity, N, is unknown. This term is also included in the phase pseudorange equation:

$$\lambda\phi = \rho + c\Delta\delta + \lambda N \tag{3.14}$$

where λ is the wavelength of the carrier signal, ρ is the geometric range, $\Delta\delta$ is the difference between clocks and c is the speed of light.

3.1.3 Ionosphere-free Linear Combination of Observations

The ionosphere is one the most influenced error sources for GNSS signals. However, the combination of different observation makes it possible to eliminate this error up to 99.9 percent (Subirana et al., 2011). Dual frequency GNSS receivers can easily combine the measurements on L1 and L2 carrier phase and generate ionosphere-free linear combination to remove ionospheric delay. This is one of the main advantages of dual frequency receivers. In precise GNSS applications, the ionosphere-free linear combination of L1 and L2 phase observations is commonly used in the data processing to remove the effects of ionospheric refraction (Hofmann-Wellenhof et al., 2007).

When a radio wave is transmitted into an ionized layer, refraction, or bending of the wave, occurs. This refraction is caused by an abrupt change in the velocity of the upper part of a radio wave as it strikes or enters a new medium. The amount of refraction that occurs depends on three main factors: (1) the density of ionization of the layer, (2) the frequency of the radio wave, and (3) the angle at which the wave enters the layer. The first order ionospheric effects on code and carrier-phase measurements depend on the inverse of squared signal frequency f (Subirana et al., 2011). Hence, it is possible with dual-frequency receivers to eliminate ionospheric effect through a linear combination of code measurements:

$$R_{iono-free} = \frac{f_1^2 R_{P_1} - f_2^2 R_{P_2}}{f_1^2 - f_2^2} \tag{3.15}$$

3.1.4 Error Sources

To enhance the accuracy of the positioning using GNSS, the errors that are introduced to the corresponding signals has to be corrected. These errors can be originated from the environment that GNSS signal travels, or from the receiver/transponder. The satellite clock errors, hardware errors and satellite orbit errors are categorized as errors that are introduced by the satellite.

The errors are generally because of time delays associated with the center of phase of the receiver/transponder clocks or travel path of the signal. The majority of the time delays occur for both code and carrier phase measurements. However some time delays such as wind-up, phase ambiguities are only present on carrier phase measurements. Also the ionospheric refraction occur as a delay in code measurements and advancing in phase measurements (Yeganehsahab, 2016).

3.2 Algorithms and Methods of Orbit Determination

Determination of satellite orbits is possible with different type of approaches. According to the need of the application or scientific mission, state parameters are estimated with respect to a dynamical model. This dynamic model does not necessarily need to include dynamic properties of the satellite since the kinematic approach uses a too simple model to be considered as a dynamic model.

3.2.1 Dynamic Orbit Determination

In this method the state parameters are estimated using an epoch-wise integration of a sophisticated state model (i.e. Eq. 3.16) for an extended arc of observation. By construction, the orbital trajectory is fully dependent on the underlying force models. Dynamic force models are used to describe the equation of motion and to propagate the satellite's center of mass position and velocity over time by numerical integration techniques.

$$\ddot{\mathbf{r}} = -\frac{GM}{\mathbf{r}^3} + \ddot{\mathbf{r}}_p(t_1, \mathbf{r}, \ddot{\mathbf{r}}, q_1, q_2, ..., q_d)\ddot{\mathbf{r}}_{ce} + \ddot{\mathbf{r}}_{co} + \ddot{\mathbf{r}}_{ro} \tag{3.16}$$

where $-\frac{GM}{\mathbf{r}^3}$ stands for law of gravitational acceleration; $\mathbf{r}$, $\dot{\mathbf{r}}$ and $\ddot{\mathbf{r}}$ are position, velocity and acceleration vectors, respectively; $\ddot{\mathbf{r}}_p$ is the perturbing forces acting on the satellite as a function of time, position, velocity and $q_1, ..., q_d$ are the dynamical parameters such as gravity coefficients, atmospheric drag, solar radiation pressure etc.; $\ddot{\mathbf{r}}_{ce}$, $\ddot{\mathbf{r}}_{co}$, $\ddot{\mathbf{r}}_{ro}$ are centrifugal, coriolis and rotational acceleration, respectively in an Earth-fixed frame. In this technique the errors of the force model are likely to increase with extended period of integration time. Hence, because of imperfect modeling of forces that act on the satellite the dynamic model is sensitive to the errors.

As real satellite trajectories are always particular solutions of an equation of motion, a dynamic orbit representation is certainly the most natural choice for modeling orbital motion. The dynamic model is sensitive to errors caused by the imperfect modeling of forces influencing the satellite (Karslioglu et al., 2017).

3.2.2 Reduced-Dynamic Orbit Determination

The accuracy of the measurements, GNSS constellation and satellite geometry are important factors that determine the accuracy of the observation models. The dynamic and reduced-dynamic precise orbit determination are done by numerical integration of the equation of motion and the variational equations. The integration is necessary for obtaining the orbit itself on one hand and partial derivatives with respect to orbital parameters on the other hand.

Pseudo-stochastic orbit modeling is a particular realization of the reduced-dynamic orbit determination technique (Jäggi and Arnold, 2017). The attribute 'pseudo' distinguishes this method from stochastic orbit modeling where a satellite trajectory is modeled as a solution of a stochastic differential equation (Jazwinski, 1970). Pseudo-stochastic orbit modeling, in contrast, introduces additional empirical parameters $P_1, ..., P_d$, subsequently referred to as pseudo-stochastic orbit parameters, to the deterministic equation of motion (Eq. 3.16)

$$\ddot{\mathbf{r}} = -\frac{GM}{\mathbf{r}^3} + \ddot{\mathbf{r}}_p(t_1, \mathbf{r}, \ddot{\mathbf{r}}, q_1, q_2, ..., q_d, P_1, ..., P_d)\ddot{\mathbf{r}}_{ce} + \ddot{\mathbf{r}}_{co} + \ddot{\mathbf{r}}_{ro} \tag{3.17}$$

In the reduce-dynamic POD, empirical acceleration parameters are used to compensate for dynamic modeling deficiencies. The imperfection in the dynamical model are handled partially with estimation of empirical forces (e.g. pseudo-stochastic pulses, piecewise constant accelerations and continuous piecewise linear accelerations) or force field parameters (Jäggi et al., 2005). Using the fact that the satellite tracks are particular solutions of equation of motion and taking the geometric advantage of the GNSS observations, Wu et al. (1991) applied a pseudo stochastic modeling as a realization for reduce-dynamic POD. The introduction of additional parameters to the equation of motion with a-priori known statistical properties in a deterministic manner is referred to as stochastic orbit modeling.

3.2.3 Kinematic Orbit Determination

The advances in the Global Navigation Satellite Systems, the increase in its geometric strength and the availability of high number of observations in receivers onboard LEO satellite make it possible to use a pure geometric approach for orbit determination. However, the simplicity of the prediction model in this approach (Kinematic OD in which the resulting orbit is independent of orbital perturbations) and the high dependency in the measurements, the prediction accuracy degrades over time. Hence, as the length of the time interval for prediction increases the accuracy of prediction decreases.

The GNSS tracking is the only approach that makes the purely kinematic precise orbit determination possible among all the geodetic orbit determination techniques such as SLR, DORIS or altimetry. In this approach the estimation of kinematic satellite positions are completely independent from the orbit altitude and forces such as gravity, solar radiation pressure and air drag. Consequently the presence of continuous GNSS tracking became an asset for kinematic orbit determination which allows this method to be as accurate as (reduced-)dynamic approach (Švehla and Rothacher, 2002). Recently the pseudo observations obtained from the precise kinematic orbit determination are used in new scientific methods for determination of gravity field parameters, validation of dynamical models and computation of atmospheric density information. The main reason that this approach gains attention unlike other methods which need to process the observations form ground IGS network is its low load of processing and simple and reliable algorithm (Li et al., 2017a).

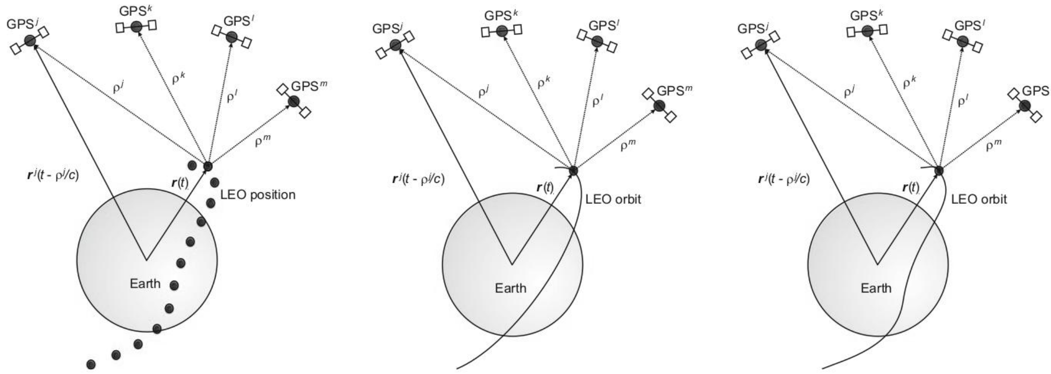

Figure 3.5: Kinematic (left), dynamic (middle), and reduced-dynamic (right) orbit representation (Jäggi and Arnold, 2017)

Kinematic orbit determination can be utilized for various type of applications since the receiver motion is not influenced by any dynamic condition. However, kinematic positions are very sensitive to erroneous measurements, poor viewing geometry, and data gaps. Kinematic positioning is therefore essentially restricted to LEO orbit determination based on spaceborne GNSS tracking data, or to GNSS orbit determination using tracking data of the terrestrial IGS ground network. Dynamic and reduced-dynamic orbit determination, in contrast, make use of physical models of the satellite motion.

The expressed orbit determination techniques can be preferred in the primary tracking systems since the major tracking systems such as SLR, can only cover an orbital arc with measurements. In the case of GNSS-based LEO orbit determination the dynamic and reduced-dynamic approaches allow for some kind of ‘averaging’ the large number of measurements from different epochs, which makes the resulting position estimates much less prone to bad measurements and data outages. Satellite trajectories can therefore be reasonably well propagated across data gaps, especially if good dynamic models are available. (Jäggi and Arnold, 2017). The representation of these orbit determination techniques are illustrated in Figure 3.5. The relation between the dynamic structure of the algorithms can be seen in the figure. The orbit path in kinematic orbit determination is drawn with dashed line while the trajectories of dynamic and reduced-dynamic methods are drawn with a continuous line which represents the dependency on dynamic model. However, the deviations from dynamic model are visible in kinematic and reduced-dynamic method since these methods can be considered as more data-driven than dynamic method.

CHAPTER 4

GNSS ORBIT SIMULATION

4.1 Overview

During last two decades, GPS-based satellite orbit determination has proven to be a solid method for satellite navigation by numerous flight missions (Montenbruck et al., 2010). Since there are upcoming constellations such as *Galileo* and *BeiDou*, as it is used for ground positioning applications, multi-constellation positioning (Multi-GNSS) became a considerable technique also for orbit determination. Compared to GPS-only positioning, it is more likely to achieve higher positioning accuracy using increased number of satellites and wide range of frequency bands. In addition to GPS measurements, Galileo measurements are simulated in this thesis by a software-defined simulator. The simulator which is developed on MATLAB 2018b consists of a set of functions to simulate the position and the velocity of both satellites and the receiver onboard the satellite. The measurements are produced by pseuodoranges modelled with respect to the signal structure and LEO environment.

In GNSS Simulation, calculated ECI satellite coordinates are converted to ECEF coordinates to be written in the ephemeris file and to be masked by the elevation angles. For the transformation between coordinate frames IERS (International Earth Rotation and Reference Systems Service) Earth Orientation Parameters are used to define precession, nutation, polar motion and earth rotation parameters. Long-term EOP data is available on IERS FTP server.

4.2 GPS and Galileo Initial Parameters

As the second constellation in addition to GPS constellation, Galileo is chosen due to its reliability (Hossam-E-Haider et al., 2014) and low-noise signal characteristics (Circiu et al., 2017; Pascual et al., 2013). A set of parameters must be defined initially to be able to obtain satellite orbits. These parameters are used in different functions in different steps which will be explained in following sections. However to start the simulation, there are some key parameters to be given such as constellation name, start date and step size. First and the most important one is the constellation name of GNSS constellations for the simulation. GPS and Galileo constellations are priori-defined in the simulation according to IGS SP3 (The Extended Standard Product 3 Orbit Format) products (Hilla, 2016) and Galileo Reference Constellation on 21 November 2016 at 00:00:00 (See Table 4.1).

Table 4.1: Galileo Orbital Parameters with reference date of 21 November 2016 00:00:00 UTC (European GNSS Service Centre, 2019)

Slot Number	Semi-major Axis (km)	Eccentricity	Inclination(deg)	RAAN (deg)	Argument of Perigee (deg)	Mean Anomaly (deg)
B05	29599.8	0.0001	56.000	77.632	0.000	15.153
B06	29599.8	0.0001	56.000	77.632	0.000	60.153
C04	29599.8	0.0001	56.000	197.632	0.000	345.153
C05	29599.8	0.0001	56.000	197.632	0.000	30.153
B08	29599.8	0.0001	56.000	77.632	0.000	150.153
B03	29599.8	0.0001	56.000	77.632	0.000	285.153
A08	29599.8	0.0001	56.000	317.632	0.000	135.153
A05	29599.8	0.0001	56.000	317.632	0.000	0.153
C07	29599.8	0.0001	56.000	197.632	0.000	120.153
C02	29599.8	0.0001	56.000	197.632	0.000	255.153
A02	29599.8	0.0001	56.000	317.632	0.000	225.153
A06	29599.8	0.0001	56.000	317.632	0.000	45.153
C06	29599.8	0.0001	56.000	197.632	0.000	75.153
C08	29599.8	0.0001	56.000	197.632	0.000	165.153
C03	29599.8	0.0001	56.000	197.632	0.000	300.153
C01	29599.8	0.0001	56.000	197.632	0.000	210.153
A03	29599.8	0.0001	56.000	317.632	0.000	270.153
A07	29599.8	0.0001	56.000	317.632	0.000	90.153
A04	29599.8	0.0001	56.000	317.632	0.000	315.153
A01	29599.8	0.0001	56.000	317.632	0.000	180.153
B04	29599.8	0.0001	56.000	77.632	0.000	330.153
B01	29599.8	0.0001	56.000	77.632	0.000	195.153
B02	29599.8	0.0001	56.000	77.632	0.000	105.153
B07	29599.8	0.0001	56.000	77.632	0.000	240.153

To define the date and time for the simulation, a UTC time must be inserted in the program. The date and time will then be converted to julian date (JD), day of year (DOY) and day of week (DOW) to be used in different outputs. Simulation step size is related to propagation step size which determines the interval to achieve position and velocity information. Propagation steps and types will be explained in the following section.

4.2.1 GNSS Kinematic Positioning for Initial Coordinates

For the determination of initial coordinates of a LEO satellite, raw observations can be used in a simple positioning algorithm. Kinematic positioning is the calculation of the position of moving receiver on the Earth or onboard the satellite (See Fig. 4.1). A *single point positioning* which is also referred to as *absolute positioning* technique is used to calculate receiver position with respect to the Earth's reference frame. At least four pseudorange measurements are required to calculate position at a time. Broadcasted satellite positions or precise GNSS satellite positions derived from precise orbit products and measured quantities are used to approximate position of the receiver with least squares method. These quantities are the distance between GNSS satellite and the receiver.

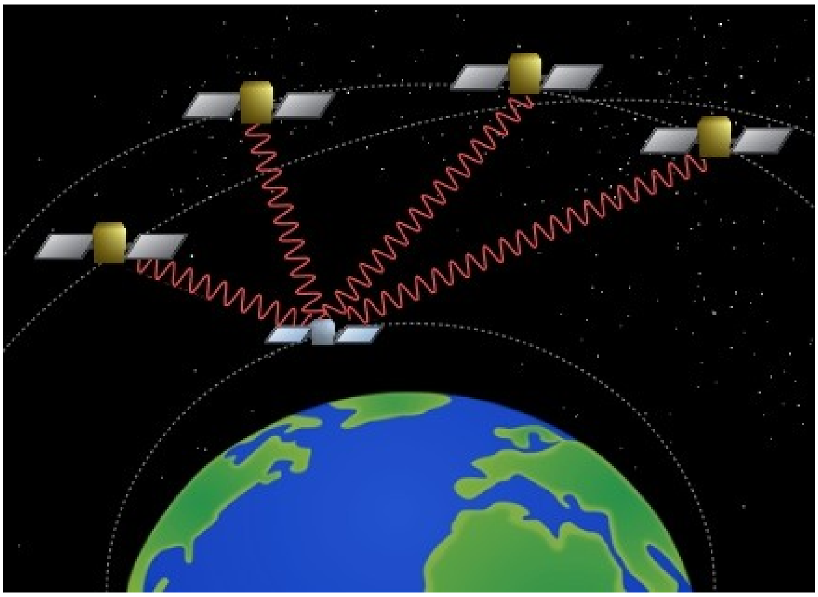

Figure 4.1: GNSS-based positioning for onboard receiver

The distance between GNSS satellites and a GNSS receiver can be calculated with different type of measurements. These measurements are called *observables* which will be explained in Section 3.1.2. These measurements are used in parameter estimation algorithms to calculate receiver position in an earth-fixed or inertial frame.

4.3 Two-step Propagation

To propagate orbital motion of a satellite, an initial position and velocity information in ECI frame is needed as an initial parameter. For propagation of these quantities numerical methods are widely used in orbital mechanics. As it is stated in the previous chapters, due to its simplicity and stability, the 4th-order Runge-Kutta (RK4) method is preferred in this thesis.

In GNSS Orbit Simulation, there are two different orbit types to be propagated; LEO satellite orbit and the orbit of GNSS satellites. The propagation of these orbits are performed in two steps. In the first step, initial state of LEO satellite with GNSS receiver is propagated with specified step size along the orbit and at each step state matrix is stored. In the second step, all the satellites for chosen constellation are propagated with the same procedure and all states are stored to be masked by their elevations according to the LEO satellite.

Although the RK4 integration is a simple and fast method, it is a coarse technique in terms of accuracy. The propagation method which is applied in this thesis, can be considered as a geometric approach which is independent of accelerations caused by various perturbations. Since the outputs of two-step propagation are assumed to be true values and are used as reference for filtered results, accuracy of the propagation with respect to the real orbit is not crucial at this point. The position differences between the geometrically propagated orbits and a reference orbit can be seen in Figure 4.2. In the different studies or applications which require accurate reference orbit, different integration methods can be used in the simulation.

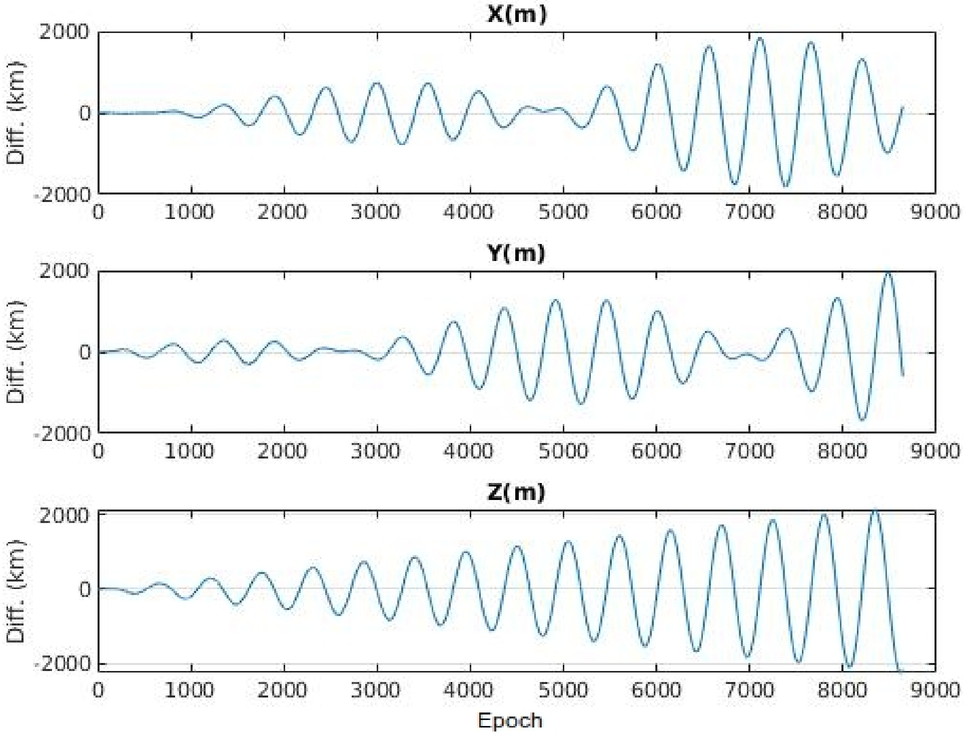

Figure 4.2: Differences between real GRACE orbit and RK4 Geometric Approach for 24h (10s interval)

4.4 Raw Data Generation

Raw data generation is the main part of the simulation. The outputs are created and formed with respect to additional constraints. In this thesis, only code pseudoranges are simulated as observations. The processes will be explained respectively in the following subsections.

4.4.1 Generation of Satellite Ephemerides

Satellite ephemerides contain position, velocity and time information at each epoch corresponding to seconds of the day. Additionally GNSS Satellite ephemerides provide calculated or defined clock error values in microseconds. A script is developed to generate IGS SP3 (The Extended Standard Product 3 Orbit Format) Ephemeris file. An example of IGS ephemeris file is shown in Fig. 4.3. The script collects all information from propagator and write them into a text file with the same structure and the order of IGS SP3s. There is a unique identification for each satellite constellation in generated ephemeris file. The intervals between the epochs are set to 15 minutes as it is in IGS products.

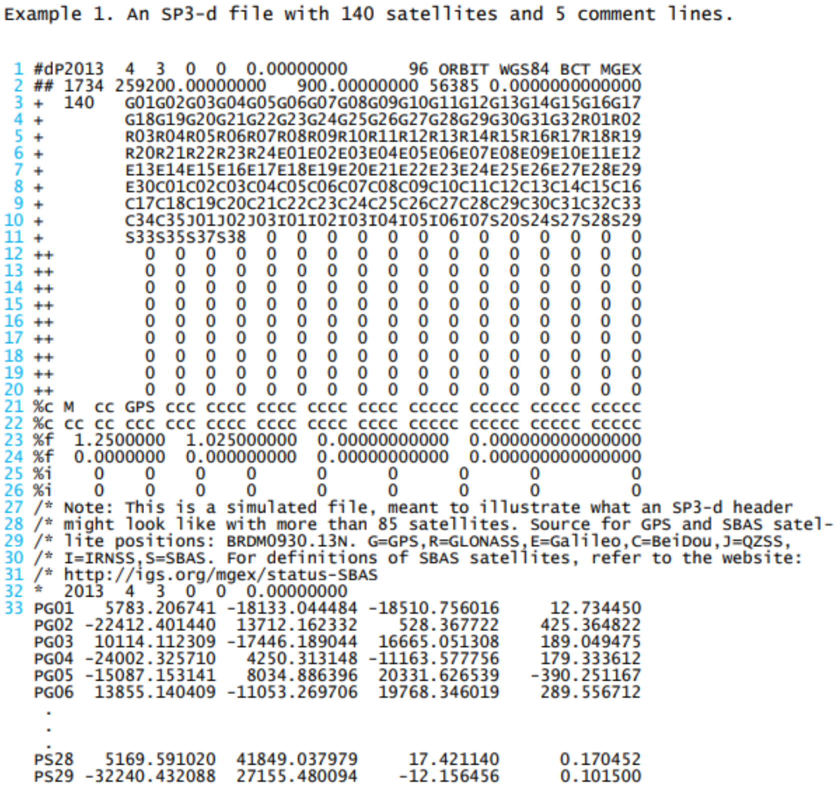

```
Example 1. An SP3-d file with 140 satellites and 5 comment lines.

#dP2013  4  3  0  0  0.00000000      96 ORBIT WGS84 BCT MGEX
## 1734 259200.00000000   900.00000000 56385 0.0000000000000
+  140   G01G02G03G04G05G06G07G08G09G10G11G12G13G14G15G16G17
+        G18G19G20G21G22G23G24G25G26G27G28G29G30G31G32R01R02
+        R03R04R05R06R07R08R09R10R11R12R13R14R15R16R17R18R19
+        R20R21R22R23R24E01E02E03E04E05E06E07E08E09E10E11E12
+        E13E14E15E16E17E18E19E20E21E22E23E24E25E26E27E28E29
+        E30C01C02C03C04C05C06C07C08C09C10C11C12C13C14C15C16
+        C17C18C19C20C21C22C23C24C25C26C27C28C29C30C31C32C33
+        C34C35J01J02J03I01I02I03I04I05I06I07S20S24S27S28S29
+        S33S35S37S38  0  0  0  0  0  0  0  0  0  0  0  0  0
++         0  0  0  0  0  0  0  0  0  0  0  0  0  0  0  0  0
++         0  0  0  0  0  0  0  0  0  0  0  0  0  0  0  0  0
++         0  0  0  0  0  0  0  0  0  0  0  0  0  0  0  0  0
++         0  0  0  0  0  0  0  0  0  0  0  0  0  0  0  0  0
++         0  0  0  0  0  0  0  0  0  0  0  0  0  0  0  0  0
++         0  0  0  0  0  0  0  0  0  0  0  0  0  0  0  0  0
++         0  0  0  0  0  0  0  0  0  0  0  0  0  0  0  0  0
++         0  0  0  0  0  0  0  0  0  0  0  0  0  0  0  0  0
++         0  0  0  0  0  0  0  0  0  0  0  0  0  0  0  0  0
%c M  cc GPS ccc cccc cccc cccc cccc ccccc ccccc ccccc ccccc
%c cc cc ccc ccc cccc cccc cccc cccc ccccc ccccc ccccc ccccc
%f  1.2500000  1.025000000  0.00000000000  0.000000000000000
%f  0.0000000  0.000000000  0.00000000000  0.000000000000000
%i    0    0    0    0      0      0      0      0         0
%i    0    0    0    0      0      0      0      0         0
/* Note: This is a simulated file, meant to illustrate what an SP3-d header
/* might look like with more than 85 satellites. Source for GPS and SBAS satel-
/* lite positions: BRDM0930.13N. G=GPS,R=GLONASS,E=Galileo,C=BeiDou,J=QZSS,
/* I=IRNSS,S=SBAS. For definitions of SBAS satellites, refer to the website:
/* http://igs.org/mgex/status-SBAS
*  2013  4  3  0  0  0.00000000
PG01   5783.206741 -18133.044484 -18510.756016     12.734450
PG02 -22412.401440  13712.162332    528.367722    425.364822
PG03  10114.112309 -17446.189044  16665.051308    189.049475
PG04 -24002.325710   4250.313148 -11163.577756    179.333612
PG05 -15087.153141   8034.886396  20331.626539   -390.251167
PG06  13855.140409 -11053.269706  19768.346019    289.556712
  .
  .
  .
PS28   5169.591020  41849.037979     17.421140      0.170452
PS29 -32240.432088  27155.480094    -12.156456      0.101500
```

Figure 4.3: IGS SP3 File Format (Hilla, 2016)

Generated ephemeris files are also one of the outputs of the simulation. These files are used later in the filtering procedure to determine LEO satellite orbits.

4.4.2 Elevation Mask

In ground positioning, generally a mask angle is defined in the receivers to eliminate some GNSS satellites with low elevation angles. The signals coming from those GNSS satellites are mostly weak and affected by the atmosphere due to long signal path. For more accurate positioning, these observations need to be removed to have a more reliable data set. This procedure is also used in GPS-based orbit determination (Bisnath and Langley, 2001) with the same principle. Using elevation mask in this simulation, not only low elevation satellites are eliminated but also satellites below horizon are prevented to be in the data set.

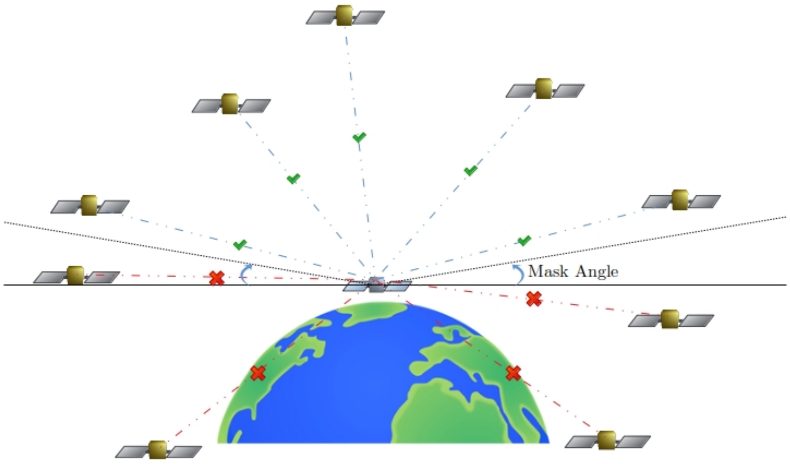

Figure 4.4: GNSS Simulation Elevation Mask

Propagated GNSS satellites are sifted out according to their elevations (See Fig. 4.4). Then, masked satellite positions are used in the calculation of geometric ranges and also in the error approximation.

The visibilities of the satellites are monitored at each epoch and Geometric Dilution of Precision (GDOP) values are calculated and stored in an array. GDOP is a term which is used to represent measurement precision according to the geometric distribution of the satellites. It can be calculated from the unit vectors between the receiver and the satellites. Let matrix $\mathbf{X}$ represents the directional derivatives of all the visible satellites form a (n × 4) matrix, $\mathbf{X}$, where n is the total number of visible satellites. In case of 4 visible satellites, $\mathbf{X}$ matrix can be formed as:

$$\mathbf{X} = \begin{bmatrix} \frac{(x_1-x)}{R_1} & \frac{(y_1-y)}{R_1} & \frac{(z_1-z)}{R_1} & -1 \\ \frac{(x_2-x)}{R_2} & \frac{(y_2-y)}{R_2} & \frac{(z_2-z)}{R_2} & -1 \\ \frac{(x_3-x)}{R_3} & \frac{(y_3-y)}{R_3} & \frac{(z_3-z)}{R_3} & -1 \\ \frac{(x_4-x)}{R_4} & \frac{(y_4-y)}{R_4} & \frac{(z_4-z)}{R_4} & -1 \end{bmatrix} \tag{4.1}$$

where R_i is

$$R_i = \sqrt{(x_i - x)^2 + (y_i - y)^2 + (z_i - z)^2} \tag{4.2}$$

where x_i, y_i, z_i and x, y, z are the position vector components for each GNSS satellites and the LEO satellite or the receiver, respectively. Taking the inverse of normal equation matrix $\mathbf{X}^T\mathbf{X}$ yields a (4 × 4) matrix where the diagonal terms gives the square of the DOP sigma values in each direction including time. The elements of the cofactor matrix $\mathbf{Q}$ which is the inverse of the normal equation matrix can be designated as follows:

$$\mathbf{Q} = (\mathbf{X}^T\mathbf{X})^{-1} = \begin{bmatrix} {\sigma^2}_x & \sigma_{xy} & \sigma_{xz} & \sigma_{xt} \\ \sigma_{xy} & {\sigma^2}_y & \sigma_{yz} & \sigma_{yt} \\ {\sigma^2}_{xz} & \sigma_{yz} & {\sigma^2}_z & \sigma_{zt} \\ {\sigma^2}_{xt} & \sigma_{yt} & \sigma_{zt} & {\sigma^2}_t \end{bmatrix} \tag{4.3}$$

PDOP, TDOP and GDOP can be calculated as:

$$\begin{aligned} PDOP &= \sqrt{{\sigma^2}_x + {\sigma^2}_y + {\sigma^2}_z} \\ TDOP &= \sqrt{{\sigma^2}_t} \\ GDOP &= \sqrt{PDOP^2 + TDOP^2} \end{aligned} \tag{4.4}$$

4.4.3 Pseudorange Calculation

Various parameters are considered to be affected on the calculation of code pseudorange measurement. The parameters are defined according to the errors which have impact on pseudorange calculation. These errors are either environmental or instrumental errors. Unlike range measurement corrections being done in positioning, in the simulation calculated delays are added to the geometric ranges as range measurement errors. To start the process, some user-defined parameters need to be defined. In satellite positioning pseudorange equation can be defined as follows:

$$p = \rho + c(dt^s - dt_r) + d_{rel} + d_{ion} + d_{trop} + d_{mp} + d_{K r} - {d_K}^s + \epsilon_P \tag{4.5}$$

where

ρ is the geometric range between the satellite and the receiver,

c is the speed of electromagnetic wave,

dt^s and dt_r are the satellite and the receiver clock offsets from the GNSS time scale,
d_{rel} is the relativistic error,
d_{ion} is the ionospheric delay,
d_{trop} is the tropospheric delay,
d_{mp} is the error due multipath,
d_{K_r} and ${d_K}^s$ are the receiver and the satellite instrumental bias,
and ϵ_P is the receiver range measurement error in terms of white noise

Code pseudorange orbservations are contaminated by all of these errors, and the raw observations need to be corrected by modeling each error. Hovever, some of these errors do not interfere with the measurements in orbit determination of LEO satellites. Since LEO satellites orbiting beyond troposphere, signals do not pass thorough the Troposphere layer. So, tropospheric delay is not an issue in LEO orbit determination. The multipath effect around LEO satellite can be also neglected due to near-earth space environment. Hence, pseudorange equation for the simulation can be formed as:

$$p = \rho + c(dt^s - dt_r) + d_{rel} + d_{ion} + \epsilon_{RN} + \epsilon \tag{4.6}$$

In the equation for the simulation, ϵ_{RN} and ϵ parameters are included to deal with random system noise errors and unmodeled random noise errors, repectively. Calculation of the pseudoranges without noise addition is explained in Figure 4.6.

4.4.3.1 Satellite and Receiver Clock Error

One of the most important priori defined parameters is clock bias parameter. In GNSS positioning clock errors always need to be calculated precisely to obtain accurate positioning information. In the simulation clock errors are added to the pseudoranges and stored in an array to be removed in the filtering procedure.

Since Galileo satellites carry Passive Hydrogen Maser (PHM) atomic clock as their main onboard clock, it is expected to provide more accurate clock information compared to atomic clocks used in GPS. The clock is made of an atomic resonator and uses hydrogen atom to measure time. The *Allan deviation* is a measure to describe frequency stability of clocks of oscillators. It is a well-known method to analyze the noise within a signal over time. Allan deviation characteristics for different clock types are given in Figure 4.5. τ symbol is the averaging period for the Allan deviation

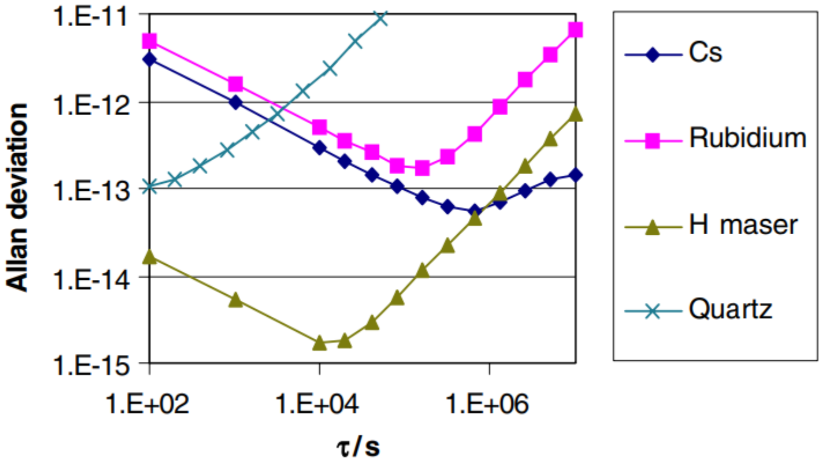

Figure 4.5: Allan deviation of high precision frequency standards (Tavella, 2008)

However in this thesis, there is no need to classify the clocks according to their performances since all of the clock errors are corrected regardlessly in the filtering procedure. Satellite clock errors either can be user-defined or can be taken from SP3 products. To define Galileo satellite clock errors, The Multi-GNSS Experiment (MGEX) SP3 products can be used. If there is no clock error information in SP3 for any satellite, then clock error will be interpolated using 1-D data interpolation with respect to the existing clock errors in SP3 file.

The clock components of GNSS receivers are the built-in quartz clocks with high frequency offsets. The quartz clocks have approximately two orders worse frequency stability when compared to rubidium atomic clocks (Yeh et al., 2009). Receiver clock bias is generally estimated along with the position and velocity parameters. For the validation of clock estimation in the filtering procedure, a priori-defined clock value can be used in the simulation. Therefore, the receiver clock error is a user-defined parameter and is directly added to the pseudoranges. User can specify the accuracy of the receiver in the simulation by this parameter.

4.4.3.2 Relativistic Error

Along with relative motion between the satellite and the receiver, post-Newtonian theory of relativity is presented as a background in numerical treating of satellite navigation relativistic effects. Due to orbit eccentricity, variations of velocity and the gravitational potential cause relativistic effects on the signal between a moving satellite with the receiver and GNSS satellite (Swatschina, 2009).

The Orbit Eccentricity Effect is a relativistic effect due to the rate of change of eccentric anomaly and it can be corrected with a clock correction term as follows:

$$d_{rel} = -2\frac{\mathbf{r}_{sat}\mathbf{v}_{sat}}{c^2} \tag{4.7}$$

where $\mathbf{r}_{sat}$ and $\mathbf{v}_{sat}$ are the satellite position and velocity vector in an inertial frame and c is the speed of light.

In the pseudorange calculation, relativistic errors ($\Delta_{rel}c$) are added to the geometric ranges to take the rate of advances of the clocks onboard the satellites into account with respect to general relativity and simulate orbital motion rigorously.

4.4.3.3 Ionosphere Error

Ionosphere can be considered as the environmental error with a greatest impact on GNSS signals. The layer is ionized by solar radiation and consists of free electrons. Ionosphere is a dispersive medium with respect to GNSS radio signals and the time delay caused by the ionosphere depends on the frequency of the signal. Ionospheric delay is a function of the Total Electron Content:

$$\Delta t_{iono} = 40.3\frac{TEC}{f^2} \tag{4.8}$$

where f is the frequency of the signal and TEC is the Total Electron Content $(1\ TECU = 10^{16}\ electrons/m^2)$ along the signal path. In this thesis, Klobuchar ionospheric model (Klobuchar, 1987) is used to calculate ionospheric time delay on each frequency. In order to calculate ionospheric delay, Klobuchar model coefficients

α and β are required. For the simulation the coefficients are taken from broadcasted GPS ephemeris file of the reference date of 21 November 2016.

According to the Klobuchar model algorithm the earth-centered angle is calculated by:

$$\psi = \frac{0.0137}{E + 0.11} - 0.022 \tag{4.9}$$

where E is the elevation of the GNSS satellite with respect to the LEO observer. The latitude of the Ionospheric Pierce Point (IPP) can be calculated as follows:

$$\phi_I = \phi_u + \psi \cos A \tag{4.10}$$

where ϕ_u is geodetic latitude and A is the azimuth of the GNSS satellite with respect to the LEO observer. If $\phi_I > 0.416$ then $\phi_I = 0.416$ and if $\phi_I < -0.416$ then $\phi_I = -0.416$. The longitude of the IPP is calculated as:

$$\lambda_I = \lambda_u + \frac{\psi sinA}{\cos \phi_I} \tag{4.11}$$

where λ_u is geodetic longitude. The geomagnetic latitude of the IPP is given as:

$$\phi_m = \phi_I + 0.064 \cos(\lambda_I - 1.617) \tag{4.12}$$

Then the local time at the IPP is computed as:

$$t = 43200\lambda_I + t_{GPS} \tag{4.13}$$

Local time t is subtracted by 86400 if $t >= 86400$. And if $t < 0$, then 86400 is added. Amplitude of ionospheric delay can be calculated as follows:

$$A_I = \sum_{n=0}^{3} \alpha_n \phi_m^n \tag{4.14}$$

where $A_I = 0$ if $A_I < 0$. Computed period of ionospheric delay is given by:

$$P_I = \sum_{n=0}^{3} \beta_n \phi_m^n \tag{4.15}$$

where $P_I = 72000$ if $P_I < 72000$. And, computed phase of ionospheric delay in radians is given by:

$$X_I = \frac{2\pi(t - 50400)}{P_I} \tag{4.16}$$

For the mean ionospheric location, slant factor is calculated by:

$$F = 1.0 + 16.0(0.53 - E)^3 \tag{4.17}$$

Then, the ionospheric time delay is computed by:

$$d_{ion_{L1}} = \begin{cases} \left[5 \times 10^{-9} + \sum_{n=0}^{3} \alpha_n \phi_m^n \left(1 - \frac{X_I^2}{2} + \frac{X_I^4}{24}\right)\right].F & |X_I| < 1.57 \\ 5 \times 10^{-9}.F & |X_I| \geqslant 1.57 \end{cases} \tag{4.18}$$

The ionospheric delay for a different frequency can be computed by:

$$d_{ion_x} = \left(\frac{f_{L1}}{f_x}\right)^2 d_{ion_{L1}} \tag{4.19}$$

4.4.3.4 System Noise

Receiver system noise can be interpreted as the measurement error of the receiver. This error directly affects the tracking performance of the GNSS receiver. The receiver synchronizes the PRN code superimposed on a modulated carrier wave received from a GPS satellite with a replica of the same code transmitted in the incoming signal to estimate the traveled distance by the received signal. In order to track the code parameters of the transmitted signal, tracking loops are used in closed loop to estimate the noise impact in the receiving signal. In this thesis, the range error due to thermal noise, antenna noise and measurement error noise are represented with Receiver System Noise Error and will be added to the geometric ranges.

Signal-to-noise ratio (SNR) is a very important factor to assess the performance of the GNSS receiver with respect to the precision of the observations. SNR is a measure used in signal processing to analyze the level of a signal compared to its background noise. The SNR of a modulated signal at radio and intermediate frequencies (RF and IF) is commonly described with carrier-to-noise-power-density ratio, C/N_0, which corresponds to the power level of a signal carrier to the noise power in a 1-Hz bandwidth. For GPS signals nominal C/N_0 values are expected to be over 45 dB-Hz and in modern receivers it is likely to experience values of 50 dB-Hz or so (Langley, 1997).

Since Galileo offers signal modulations such as BOC (Binary Offset Carrier) and AltBOC (Alternative BOC modulation), the E5a and E5b bands can be either

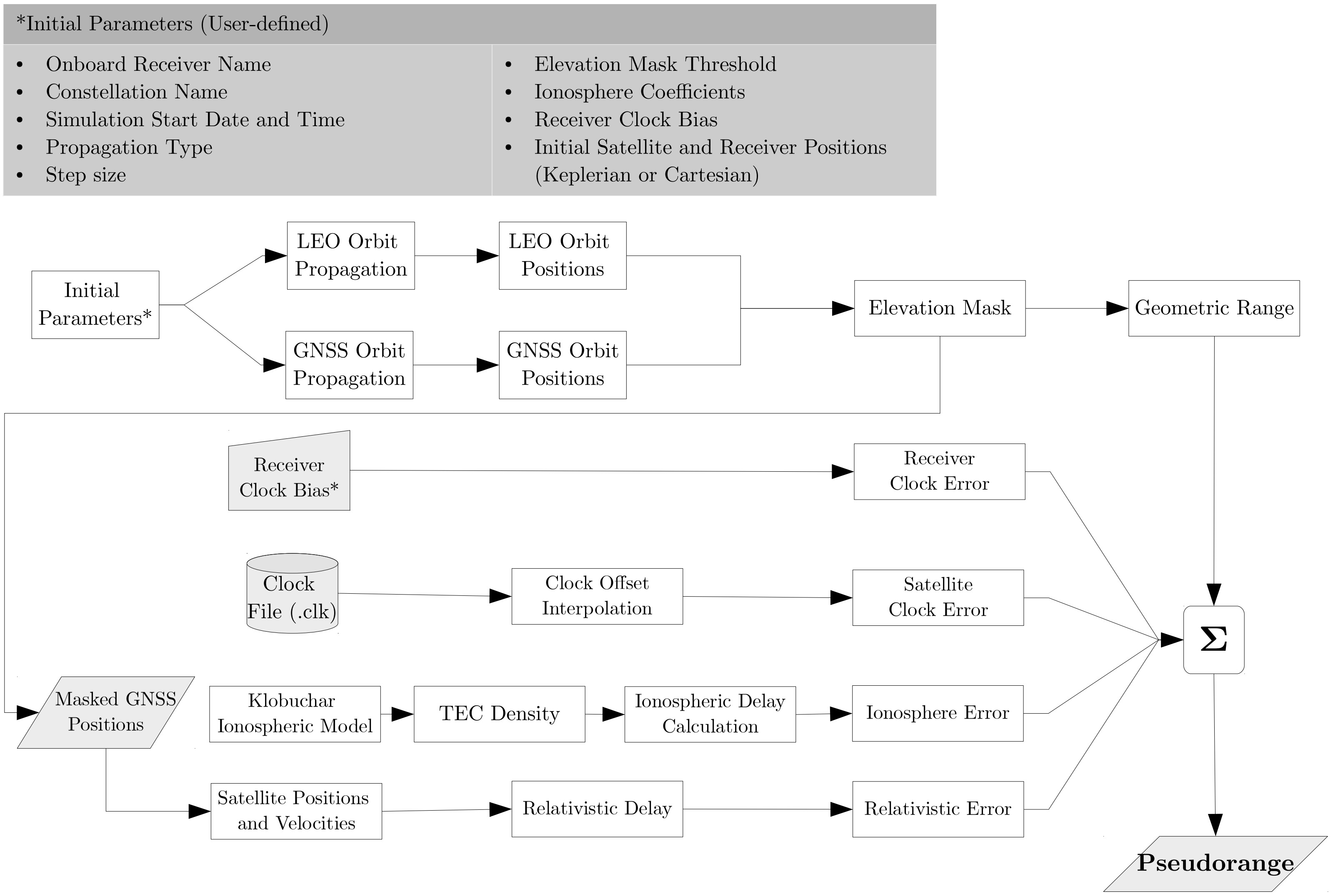

Figure 4.6: Pseudorange Calculation

processed independently as conventional BPSK (10) signals or processed together. This allows Galileo signals huge performance improvements in terms of tracking noise (Sleewaegen et al., 2004).

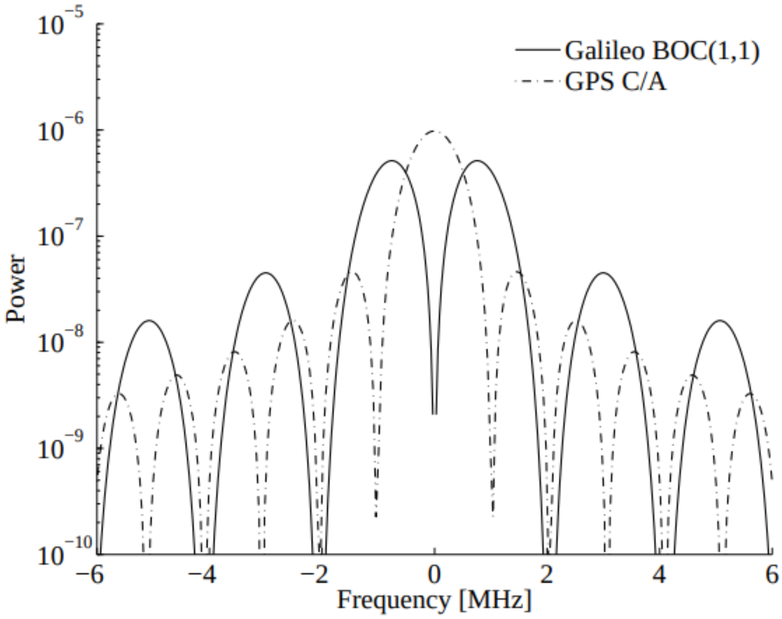

Figure 4.7: GPS C/A and Galileo BOC(1,1) sharing the L1/E1 spectrum. The center frequency is 1575.42 MHz (Borre, 2009)

It can be seen in Figure 4.7 that using higher frequency components on signal multiplexing broadens the power spectral density (PSD) spectrum for BOC modulated signals. Using spreading codes higher sample rates with larger bandwidths, possibly increase the accuracy (Sarnadas and Ferreira, 2011).

To determine the tracking performance of the GNSS receiver C/N_0 values are approximated with respect to the elevation angles of the satellites. Then, C/N_0 values are used in code-tracking loop to estimate the range errors due to receiver noise. The code-tracking loop or *delay lock loop* (DLL) jitter for an early/late one-chip-spacing correlator can be calculated as follows:

$$\sigma_{DLL} = \sqrt{\frac{\alpha B_L d}{c/n_0}\left[1 + \frac{2}{T \;\, c/n_0}\right]}\,\lambda_c \tag{4.20}$$

where α is the dimensionless DLL discriminator correlator factor, chosen as 0.5 for dedicated early/late correlator; B_L is the code loop noise bandwidth in Hz, chosen

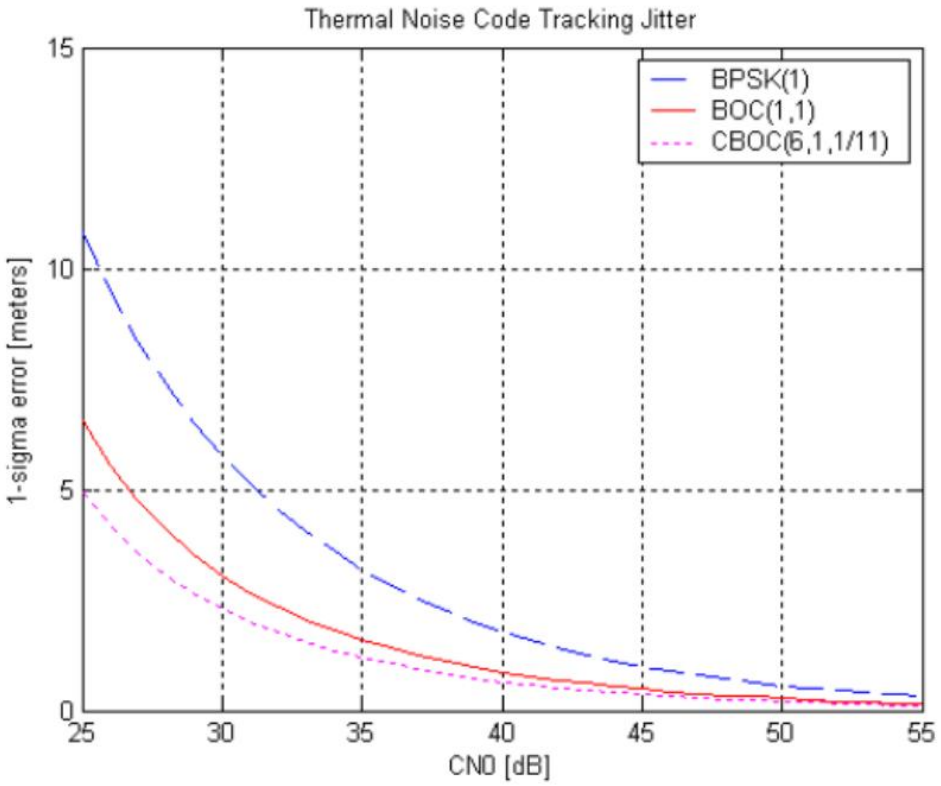

Figure 4.8: GPS C/A BPSK(1), Galileo BOC(1,1) and Galileo CBOC(6,1,1/11) code tracking errors (Sarnadas and Ferreira, 2011)

as 0.8, c/n_0 is the carrier-to-noise density ratio in dB-Hz $(c/n_0 = 10^{\frac{C/N_0}{10}})$, T is the predetection integration time in seconds, chosen as 0.02; λ_c is the wavelength of the PRN code, given as 293.05 m for C/A code and 29.305 m P code; and d is correlator spacing in chips, chosen as 0.1 in the simulation. Code tracking error is related to chip width. Therefore, when compared to P code solution, it is expected to deal with larger errors in C/A code solution. In the new generation GNSS receivers, the narrow correlator spacing in chips are used. Using less than one chip reduces the error in code tracking and allows more accurate solution.

By taking previous research and studies (Hauschild et al., 2014; Pany et al., 2003; Eissfeller et al., 2007) into consideration minimum C/N_0 values are selected as 34 for GPS and 38 for Galileo with respect to the signal powers and typical C/N_0 values for each constellation. 1-sigma errors related to C/N_0 values for different modulation processes can be seen in Figure 4.8. For a Galileo satellite transmitting the signal at

E deg of elevation receiver system noise error is calculated as:

$$C/N_0 = C/N_{0_{min}} + 0.235294117647059(E - 5) \tag{4.21}$$

where $C/N_{0_{min}}$ is priori-defined the minimum carrier-to-noise-density ratio that can be achieved with respect to the constellation and E is the elevation of GNSS satellite. Code tracing error is calculated with substituting C/N_0 values in the equation 4.20. Then, receiver system noise error is calculated by:

$$\epsilon_{RN} = \sigma_{DLL} \;.\; \mathrm{RND}[0:1] \tag{4.22}$$

where $\mathrm{RND}[0:1]$ is a random number generated between 0 and 1.

In addition to the receiver system noise error, to cope with the errors from unknown sources an unmodeled random noise term $\epsilon = \mathrm{RND}[0:0.1]$ m is added to the pseudorange calculation. This error is the result of random noise which is also dependent on satellite elevation. Errors caused by random noise are not estimated as a parameter in the filtering procedure. However, it is possible to observe the filter behavior in the presence of random noise contaminate the pseudorange measurements.

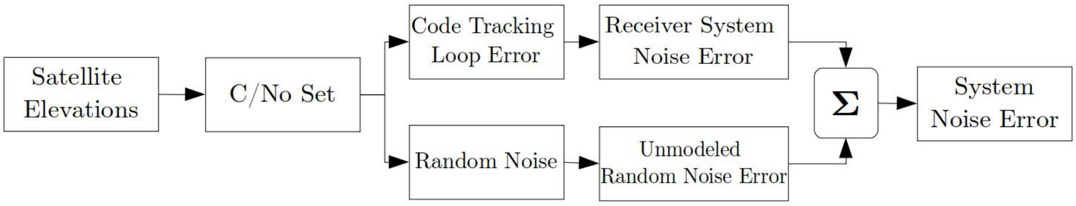

Figure 4.9: System Noise Errors

System noise errors are added to the pseudoranges before the filtering procedure. Calculation of system noise errors with respect to satellite elevation is expressed in Figure 4.9.

4.4.3.5 True LEO Orbit

In order to compute the true orbit of a LEO satellite, calculated pseudoranges are used in an analytical calculation of LEO orbits. Cartesian coordinates of LEO satellite are calculated with true range multilateration. Calculated pseudoranges from four available satellite setup with the best GDOP value are used in the solution of the simple geometry problem.

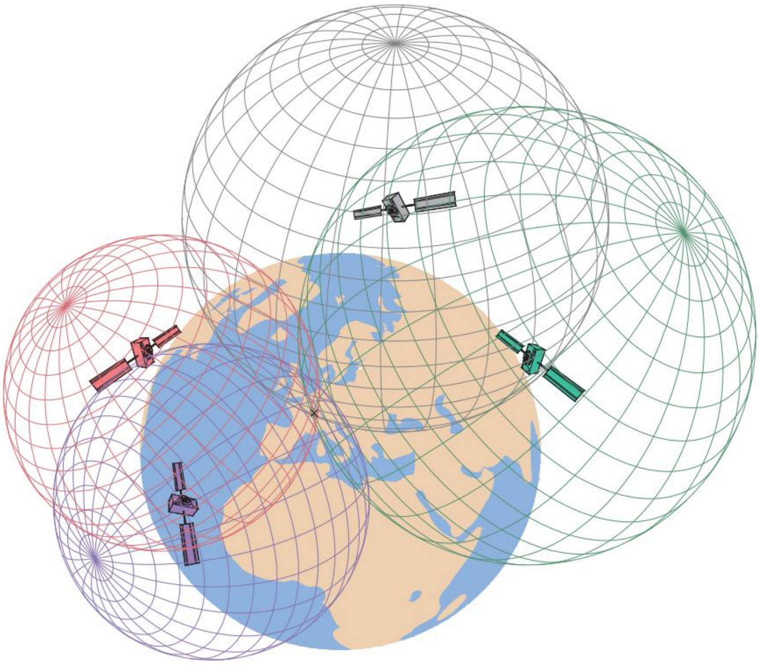

Figure 4.10: GNSS Trilateration (Peyret et al., 2015)

True range multilateration is a mathematical technique to calculate the position of a moving or a stationary object fundamentally by finding the intersection of a series of spheres. Using multiple ranges from spatially-separated known points, another point in space can be calculated. True range multilateration, often called *trilateration* method is practically applied in surveying for a solution of a simple geometry problem of a fixed location. It is commonly preferred cost-effective positioning technique for surveying applications. However, this simple method is extended to satellite navigation which requires the determination of time in addition to the position (Fang, 1986). Trilateration used in GNSS is illustrated with four satellites in Figure 4.10.

In order to solve 3-D cartesian trilateration problem, various algorithms, e.g. Fang (1986), Sirola (2010) and Bancroft (1985), were developed in the past for particular applications.

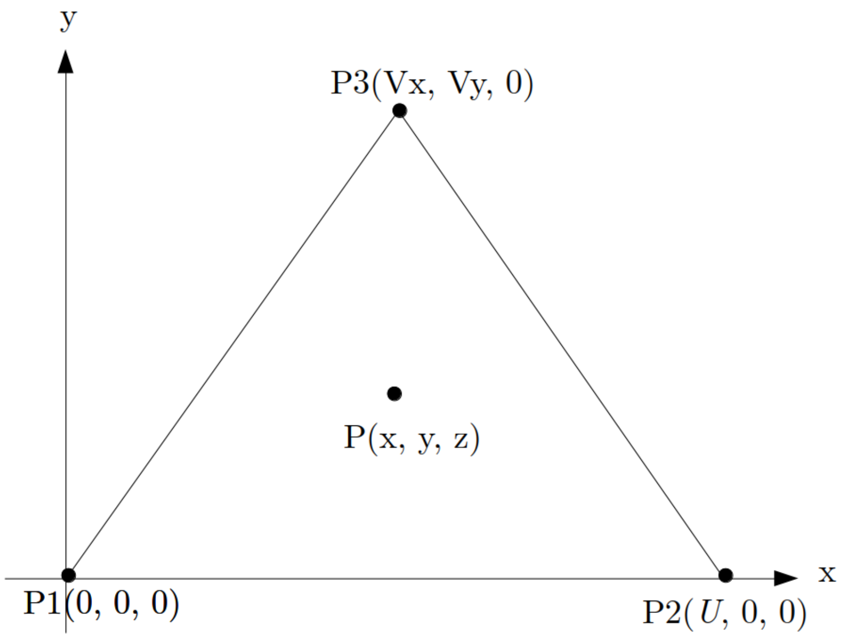

Figure 4.11: 3-D trilateration scenario

According to the scenario in Fig. 4.11, sphere centers corresponds to P1, P2 and P3 points represented on a x, y plane. If P is the position of an unknown point at (x, y, z), then Pythagoras's theorem yields the slant ranges between P and the sphere centers:

$$\begin{aligned} r_1^2 &= x^2 + y^2 + z^2 \\ r_2^2 &= (x - U)^2 + y^2 + z^2 \\ r_3^2 &= (x - V_x)^2 + (y - V_y)^2 + z^2 \end{aligned} \tag{4.23}$$

where P is the point to be calculated, P1, P2 and P3 are known centers of spheres in the x,y plane. Thus, letting $V^2 = V_x^2 + V_y^2$, the coordinates of P are:

$$\begin{aligned} x &= \frac{r_1^2 - r_2^2 + U^2}{2U} \\ y &= \frac{r_1^2 - r_3^2 + V^2 - 2V_x x}{2V_y} \\ z &= \pm\sqrt{r_1^2 - x^2 - y^2} \end{aligned} \tag{4.24}$$

In GNSS simulation, a mathematical technique is used in trilateration process for the calculation of LEO positions from produced pseudorange quantities by GNSS satellite propagation. These LEO positions are used for the comparison of proposed algorithms and applied techniques.

4.4.3.6 Outliers

Due to sensor malfunction, it is likely to see outliers in the observation data set. These outliers are needed to be either excluded from the data set or weighted with robust algorithms. In case of having limited number of measurements, removing data can cause the system to become under-determined. Since the filtering algorithm is very dependent on the observations in this thesis, outliers are weighted instead of being removed from the data set.

Calculated pseudoranges are not generated from a sensor. Therefore, the observations are free of outliers when the pseudorange calculation is completed. However, to simulate sensor malfunction and to analyze the performance of robust filter random outliers added to the observations. During three epochs single range measurement in a data set is contaminated by outliers. Three levels of outlier impact are defined as 10, 100 and 1000 km for each epoch chosen to be contaminated. The outliers are added to the observations before generating Receiver Independent EXchange (RINEX) observation files. The performance of the robust filter on the outliers will be evaluated in the Chapter 6.

4.4.4 RINEX Generation

Receiver Independent Exchange Format (RINEX) is a data format includes raw satellite navigation data. Raw measurements along with time information is provided by this file to be post-processed by the user to obtain more accurate position. Produced code pseudoranges by the simulation are written into a text file with the same format of RINEX 2.20 (Gurtner and Estey, 2013) which is a special version developed within the IGS LEO projects for space-borne GNSS receivers.

The script generates RINEX observation file (e.g. .16o) to be used as an input in the filtering procedure. Along with SP3 file generated from the simulation observation

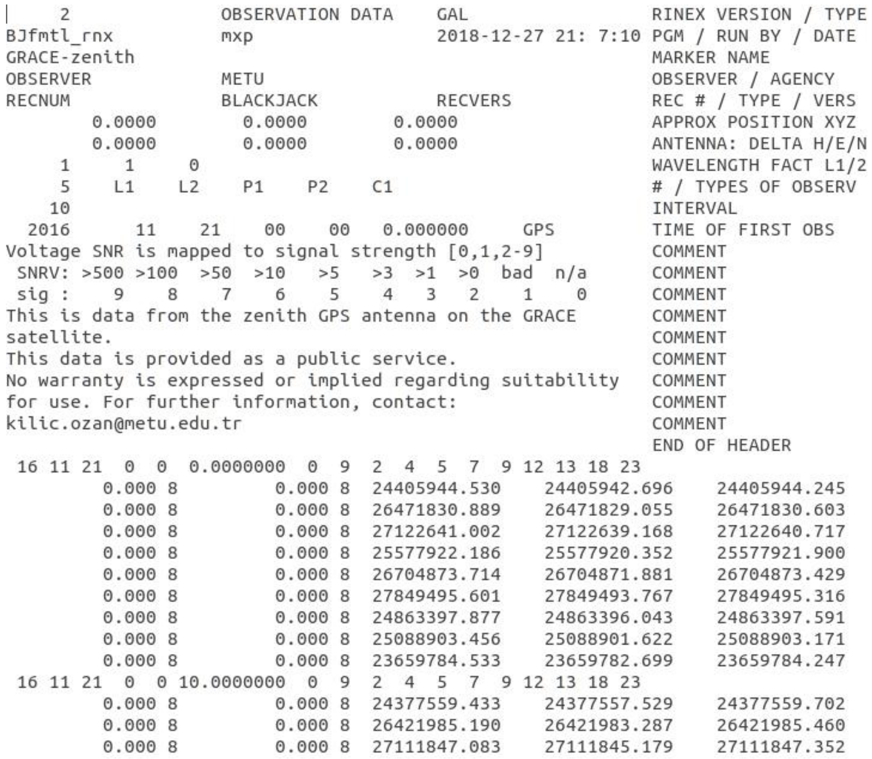

```
     2              OBSERVATION DATA    GAL                 RINEX VERSION / TYPE
BJfmtl_rnx          mxp                 2018-12-27 21: 7:10 PGM / RUN BY / DATE
GRACE-zenith                                                MARKER NAME
OBSERVER            METU                                    OBSERVER / AGENCY
RECNUM              BLACKJACK           RECVERS             REC # / TYPE / VERS
        0.0000        0.0000        0.0000                  APPROX POSITION XYZ
        0.0000        0.0000        0.0000                  ANTENNA: DELTA H/E/N
     1     1     0                                          WAVELENGTH FACT L1/2
     5    L1    L2    P1    P2    C1                        # / TYPES OF OBSERV
    10                                                      INTERVAL
  2016      11    21    00    00   0.000000     GPS         TIME OF FIRST OBS
Voltage SNR is mapped to signal strength [0,1,2-9]          COMMENT
 SNRV: >500 >100  >50  >10   >5   >3  >1  >0  bad  n/a      COMMENT
 sig :    9    8    7    6    5    4   3   2    1    0      COMMENT
This is data from the zenith GPS antenna on the GRACE       COMMENT
satellite.                                                  COMMENT
This data is provided as a public service.                  COMMENT
No warranty is expressed or implied regarding suitability   COMMENT
for use. For further information, contact:                  COMMENT
kilic.ozan@metu.edu.tr                                      COMMENT
                                                            END OF HEADER
 16 11 21  0  0  0.0000000  0  9  2  4  5  7  9 12 13 18 23
         0.000 8         0.000 8  24405944.530    24405942.696    24405944.245
         0.000 8         0.000 8  26471830.889    26471829.055    26471830.603
         0.000 8         0.000 8  27122641.002    27122639.168    27122640.717
         0.000 8         0.000 8  25577922.186    25577920.352    25577921.900
         0.000 8         0.000 8  26704873.714    26704871.881    26704873.429
         0.000 8         0.000 8  27849495.601    27849493.767    27849495.316
         0.000 8         0.000 8  24863397.877    24863396.043    24863397.591
         0.000 8         0.000 8  25088903.456    25088901.622    25088903.171
         0.000 8         0.000 8  23659784.533    23659782.699    23659784.247
 16 11 21  0  0 10.0000000  0  9  2  4  5  7  9 12 13 18 23
         0.000 8         0.000 8  24377559.433    24377557.529    24377559.702
         0.000 8         0.000 8  26421985.190    26421983.287    26421985.460
         0.000 8         0.000 8  27111847.083    27111845.179    27111847.352
```

Figure 4.12: RINEX observation file generated by the simulation

file is the output of the simulation. The RINEX observation file generated from GNSS simulation is shown in Figure 4.12.

CHAPTER 5

ADAPTIVE ROBUST KALMAN FILTERING

Two types of estimation methods are mainly used to estimate the state parameters in orbit determination: batch least squares and recursive estimation. Although both methods aim to minimize the errors, they have different working principles to be used in different types of applications. Due to its batch structure, batch processing is mainly used for post-processing applications and requires computers with high-level performance as it brings more computational loads. In real-time applications, recursive estimators are used to estimate the state parameters without storing all the data and observations (Keil, 2014). The state parameters and their covariances are estimated recursively over time using estimated parameters and their covariances from previous epoch as the input. It is very important to use rapid algorithms in continuous applications such as satellite navigation and autonomous control systems. In this thesis, the Kalman Filter is applied to estimate state parameters. It is a recursive algorithm which will be explained in the following section.

5.1 Kalman Filter

Kalman filter is a recursive algorithm which is developed by Rudolf E. Kalman. Due to its recursive structure, Kalman Filter is widely applied in orbit determination. The algorithm comprises two main steps called "Prediction" and "Correction". In the prediction step, state parameters and their zero mean Gaussian noises are transferred to the next epoch with system dynamics. This step is also called "Time Update" in the algorithm. When the measurements are obtained, the prediction with a level of uncertainty is corrected with the measurements using the weighted average.

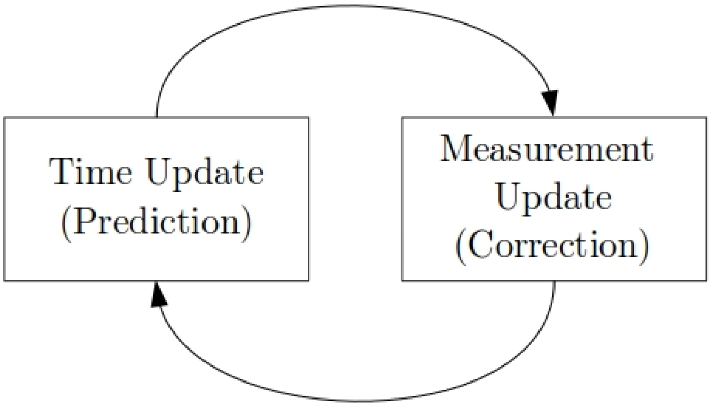

Figure 5.1: Two Step Calculation

Linear dynamic system in state space form is expressed as:

$$\dot{\mathbf{x}} = \mathbf{F}\mathbf{x} + w(t) \tag{5.1}$$

where $\mathbf{x}$ is the state vector, $\mathbf{F}$ is the dynamic (state) matrix and w is the process or system noise for the state vector components. For a dynamic nonlinear system model, a linearization procedure is needed. This can be done by Taylor series approximation:

$$\mathbf{x}_{k+1} = \mathbf{x}_k + \dot{\mathbf{x}}_k \Delta t + \ddot{\mathbf{x}}_k \frac{\Delta t}{2!} + \dots \tag{5.2}$$

According to the dynamic model, the discrete equation can be formed as:

$$\mathbf{x}_{k+1} = \mathbf{x}_k + \mathbf{F}\mathbf{x}_k \Delta t + \mathbf{F}^2 \mathbf{x}_k \frac{\Delta t^2}{2!} + \dots \tag{5.3}$$

The dynamic matrix, $\mathbf{F}$, can be carried to the next step either with State Transition Matrix (Φ) or with numerical integration which is explained in Section 2.3. The state prediction is expressed as:

$$\mathbf{x}_{k+1} = \mathbf{\Phi}_k \mathbf{x}_k \tag{5.4}$$

And the state transition matrix is derived from Eq. 5.3 as follows:

$$\mathbf{\Phi}_k = \mathbf{I} + \mathbf{F}\Delta t + \mathbf{F}^2 \frac{\Delta t^2}{2!} + \dots \tag{5.5}$$

where **I** is unit matrix. The discrete-time dynamic system can be written as:

$$\mathbf{x}_{k+1} = \mathbf{\Phi}_k \mathbf{x}_k + \omega_k \tag{5.6}$$

If state vector components are position (x, y, z) and velocity (v_x, v_y, v_z), then, the dynamic matrix **F** can be written as:

$$\mathbf{F} = \begin{bmatrix} \frac{\partial v_x}{\partial x} & \frac{\partial v_x}{\partial y} & \frac{\partial v_x}{\partial z} & \frac{\partial v_x}{\partial v_x} & \frac{\partial v_x}{\partial v_y} & \frac{\partial v_x}{\partial v_z} \\ \frac{\partial v_y}{\partial x} & \frac{\partial v_y}{\partial y} & \frac{\partial v_y}{\partial z} & \frac{\partial v_y}{\partial v_x} & \frac{\partial v_y}{\partial v_y} & \frac{\partial v_y}{\partial v_z} \\ \frac{\partial v_z}{\partial x} & \frac{\partial v_z}{\partial y} & \frac{\partial v_z}{\partial z} & \frac{\partial v_z}{\partial v_x} & \frac{\partial v_z}{\partial v_y} & \frac{\partial v_z}{\partial v_z} \\ \frac{\partial a_x}{\partial x} & \frac{\partial a_x}{\partial y} & \frac{\partial a_x}{\partial z} & \frac{\partial a_x}{\partial v_x} & \frac{\partial a_x}{\partial v_y} & \frac{\partial a_x}{\partial v_z} \\ \frac{\partial a_y}{\partial x} & \frac{\partial a_y}{\partial y} & \frac{\partial a_y}{\partial z} & \frac{\partial a_y}{\partial v_x} & \frac{\partial a_y}{\partial v_y} & \frac{\partial a_y}{\partial v_z} \\ \frac{\partial a_z}{\partial x} & \frac{\partial a_z}{\partial y} & \frac{\partial a_z}{\partial z} & \frac{\partial a_z}{\partial v_x} & \frac{\partial a_z}{\partial v_y} & \frac{\partial a_z}{\partial v_z} \end{bmatrix} \tag{5.7}$$

In Kalman Filter, error covariances are transferred to the next epoch separately with:

$$\mathbf{P}_{k+1} = \mathbf{\Phi}_k \mathbf{P}_k \mathbf{\Phi}_k^T + \mathbf{Q}_k \tag{5.8}$$

where **Q** is the noise covariance matrix of system parameters. The expected value of **Q** is given by:

$$\mathbf{Q} = \mathbb{E}(ww^T) \tag{5.9}$$

Q is a positive definite diagonal matrix consisting of noise variances of state parameters. Determination of **Q** matrix is very effective on the filter performance. While a filter with a large **Q** is overdependent on the measurements, a filter with a small **Q** is overdependent on the system model. In highly nonlinear system applications, determination of system changes is very important. In such systems, the noise covariance matrix of system noise is calculated adaptively. A filter with an adaptive estimation of noise covariances is called an *Adaptive Filter*. Adaptive filters will be explained in Section 5.4.

As a part of system equations, measurement model is given as:

$$\mathbf{z} = \mathbf{H}\mathbf{x} + \mathbf{v} \tag{5.10}$$

where **z** is the observation vector and **H** is the measurement sensitivity (design) matrix and v is the measurement (sensor) noise for the observations. The design matrix is given by:

$$\mathbf{H}_{N\times 6} \equiv \left[\left(\frac{\partial \rho_r^s}{\partial \mathbf{r}}\right)_{N\times 3} \quad \left(\frac{\partial \rho_r^s}{\partial \dot{\mathbf{r}}}\right)_{N\times 3} \right] \tag{5.11}$$

where ρ_r^s is the pseudorange observations from satellite to receiver and N is the number of observations. Corrected state vector can be determined by:

$$\hat{\mathbf{x}}_{k+1} = \bar{\mathbf{x}}_{k+1} + \mathbf{K}_{k+1}[\mathbf{z} - \mathbf{H}_{k+1}\bar{\mathbf{x}}_{k+1}] \tag{5.12}$$

where $\hat{\mathbf{x}}$ is the estimated state vector, $\mathbf{K}$ is the *Kalman Gain*, $\bar{\mathbf{x}}$ is the predicted state vector which is previously expressed in the prediction step as $\mathbf{x}_{k+1}$. Kalman gain can be calculated by:

$$\mathbf{K}_{k+1} = \bar{\mathbf{P}}_{k+1}\mathbf{H}_{k+1}(\mathbf{H}_{k+1}\bar{\mathbf{P}}_{k+1}\mathbf{H}_{k+1}^T + \mathbf{R}_k)^{-1} \tag{5.13}$$

where $\bar{\mathbf{P}}_{k+1}$ is predicted error covariance matrix, which is previously expressed in the prediction step as $\mathbf{P}_{k+1}$ and $\mathbf{R}_k$ is the measurement noise covariance matrix which is also a positive definite diagonal matrix which consists of noise variances of measurements. $\mathbf{R}_k$ matrix can be determined if the accuracy of the measurement sensor is known. It is challenging to set an optimal noise covariance without the knowledge of the sensor error. There are some robust estimation methods which include measurement covariance tuning according to the residual errors. Robust estimation will be explained in detail in Section 5.3.

Estimated error covariance matrix of state parameters, $\hat{\mathbf{P}}_{k+1}$, can be calculated as:

$$\hat{\mathbf{P}}_{k+1} = (\mathbf{I} - \mathbf{K}_{k+1}\mathbf{H}_{k+1})\bar{\mathbf{P}}_{k+1} \tag{5.14}$$

The equations of essential Kalman filter algorithm are summarized in Table 5.1. Essential Kalman Filter algorithm is generally used in the applications which the state space equation represents a linear problem. However, most of the problems in real world cannot be considered as linear. The state space equations of these problems are nonlinear differential equations. As it is stated earlier in this section, a linearization procedure has to be performed in order to to apply Kalman Filter in nonlinear systems. If the nominal estimate of the state is used to define both dynamic and measurement model functions, the algorithm is called *Linearized Kalman Filter*. This can be considered as the simplest approach to Kalman filtering for nonlinear systems, since it uses linearization of the system model about a nominal trajectory. This approach can be used in preliminary system analysis phase of the various mission scenarios with several potential trajectories (Grewal et al., 2013).

If corrected state estimate is used in each step for linearization, the algorithm is called *Extended Kalman Filter* which is a widely used extension of Kalman Filter. In this thesis, the Extended Kalman Filter (EKF) algorithm is implemented. The algorithm will be explained in the following section.

Table 5.1: Kalman Filter Algorithm

Time Update (Prediction)	
$\bar{\mathbf{x}}_{k+1} = \mathbf{\Phi}_k \mathbf{x}_k$	Predicted State Vector
$\bar{\mathbf{P}}_{k+1} = \mathbf{\Phi}_k \mathbf{P}_k \mathbf{\Phi}_k^T + \mathbf{Q}_k$	Predicted Error Covariance Matrix
Measurement Update (Correction)	
$\mathbf{K}_{k+1} = \bar{\mathbf{P}}_{k+1} \mathbf{H}_{k+1} (\mathbf{H}_{k+1} \bar{\mathbf{P}}_{k+1} \mathbf{H}_{k+1}^T + \mathbf{R}_k)^{-1}$	Kalman Gain
$\hat{\mathbf{x}}_{k+1} = \bar{\mathbf{x}}_{k+1} + \mathbf{K}_{k+1} [\mathbf{z} - \mathbf{H}_{k+1} \bar{\mathbf{x}}_{k+1}]$	Corrected State Vector
$\hat{\mathbf{P}}_{k+1} = (\mathbf{I} - \mathbf{K}_{k+1} \mathbf{H}_{k+1}) \bar{\mathbf{P}}_{k+1}$	Corrected Error Covariance Matrix

5.2 Extended Kalman Filter

Linearization is a very important part of the Kalman Filter for nonlinear applications. The Extended Kalman Filter (EKF) provides an efficient linearization performance. Thus, it is one of the most preferred algorithms for nonlinear estimation problems. Unlike the linearized version of classical Kalman Filter equations, EKF makes use of estimated state of each epoch for linearization (See Fig. 5.2). This allows state estimation to be more accurate.

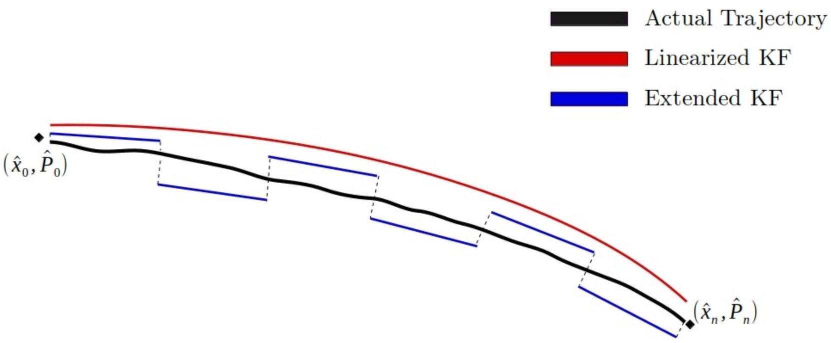

Figure 5.2: LKF and EKF representation

In the Extended Kalman Filter, the reference trajectory is updated at each epoch after measurements are processed. Integration step size between measurement epochs has to be taken small to reduce the effect of linearization error. The performance of the filter depends on the system model as well as the quality of the measurements. Additionally, an incorrect estimation of the initial state and initial error covariance can lead to the divergence of the filter. The equations of Extended Kalman Filter algorithm are summarized in Table 5.2.

Table 5.2: Extended Kalman Filter Algorithm

Time Update (Prediction)	
$\bar{\mathbf{x}}_{k+1} = \mathbf{x}_k + \int_{t_k}^{t_{k+1}} f(\mathbf{x}, t)dt$	Predicted State Vector
$\mathbf{F} = \frac{\partial \mathbf{f}}{\partial \mathbf{x}}\Big\vert_{\mathbf{x}=\hat{\mathbf{x}}(t)}$	Dynamic Matrix
$\bar{\mathbf{P}}_{k+1} = \mathbf{\Phi}_k \mathbf{P}_k \mathbf{\Phi}_k^T + \mathbf{Q}_k$	Predicted Error Covariance Matrix
Measurement Update (Correction)	
$\mathbf{K}_{k+1} = \bar{\mathbf{P}}_{k+1}\mathbf{H}_{k+1}(\mathbf{H}_{k+1}\bar{\mathbf{P}}_{k+1}\mathbf{H}_{k+1}^T + \mathbf{R}_k)^{-1}$	Kalman Gain
$\mathbf{H}_k = \frac{\partial \mathbf{h}}{\partial \mathbf{x}}\Big\vert_{\mathbf{x}=\hat{\mathbf{x}}}$	Design Matrix
$\hat{\mathbf{x}}_{k+1} = \bar{\mathbf{x}}_{k+1} + \mathbf{K}_{k+1}[\mathbf{z} - \mathbf{H}_{k+1}\bar{\mathbf{x}}_{k+1}]$	Corrected State Vector
$\hat{\mathbf{P}}_{k+1} = (\mathbf{I} - \mathbf{K}_{k+1}\mathbf{H}_{k+1})\bar{\mathbf{P}}_{k+1}$	Corrected Error Covariance Matrix

Extended Kalman Filter is very useful for space-based continuous applications but it is difficult to implement the technique in orbit determination (Vallado, 2001). Considering the noise characteristics as zero-mean Gaussian (white) noise is not always the best option to represent the real conditions of the signal environment since the power spectral density of the noise may not be uniform across the frequency spectrum. This type of frequency-dependent noise can be called colored noise. Since the Kalman Filter usually requires white noise, modeling correlated noise is only possible with a *shaping filter*. Colored noise can be generated from a white noise passing through a shaping filter (commonly a low pass filter) (Viswanathan, 2013). In this thesis, the noise is assumed as white noise in the filtering process.

As it is explained in Section 5.1, determination of noise covariance matrices Q and R is challenging all by itself. Optimal determination of these matrices may be possible with adaptive and robust estimators. These techniques will be explained further in the Section 5.3 and Section 5.4.

5.3 Robust Estimation

In the parameter estimation process, measurements which are obtained from the sensor must be checked in terms of quality. The observations can contain outliers as a result of the sensor malfunctioning. An outlier is an erratic observation which has an abnormal distance from other values in an observation sample. Generally, the outliers are needed to be excluded from the data set to prevent incorrect state estimation. However in case of having limited number of measurements, removing data can cause the system to become under-determined. This is not the most efficient way to estimate parameters for the applications which are highly dependent on the observations. Kinematic orbit determination is an example of such applications.

In robust algorithms, outliers are weighted with the equivalent measurement noise covariance matrix instead of being removed from the data set. Numerous methods are proposed in the literature to calculate equivalent measurement noise covariance matrix such as Huber weight function (Huber and Ronchetti, 1981), Hampel function, Tukey bi-weight function (Hampel et al., 2011) or IGGIII (Institute of Geodesy and Geophysics) (Yang et al., 2002) function. In this thesis, M estimation based IGGIII function is adopted to control abnormal measurements and to obtain equivalent measurement noise covariance matrix. $\mathbf{R}$ can be tuned as follows:

$$\bar{\mathbf{R}}_{k_i} = \mathbf{R}_{k_i}/\gamma_{k_i} \tag{5.15}$$

where $\bar{\mathbf{R}}_{k_i}$ is tuned measurement noise covariance matrix divided by variance inflation factor γ_{k_i} which can be calculated with IGGIII function as follows:

$$\gamma_{k_i} = \begin{cases} 1 & |\widehat{e}_i| \leqslant k_0 \\ \frac{k_0}{|\widehat{e}_i|}\left(\frac{k_1-|\widehat{e}_i|}{k_1-k_0}\right) & k_1 < |\widehat{e}_i| < k_1 \\ \approx 0 & |\widehat{e}_i| > k_1 \end{cases} \tag{5.16}$$

where $\widehat{e}_i$ standardized residuals computed from estimated residuals, k_0 and k_1 are the constants can be chosen as k_0 = 1.5 - 3.0 and k_1 = 3.0 - 5.0 according to trial-and-error based evaluation results. IGGIII function consists of three cases concerning the given threshold constants which are chosen according to experimental results. In order to prevent equivalent variance going to infinite, variance inflation factor can be set to the machine epsilon in case of measurement residual, which is too large to be accepted.

In the parameter estimation procedure, estimated residuals are calculated with corrected observations as follows:

$$\widehat{\mathbf{e}} = [\mathbf{y} - \widehat{\mathbf{y}}] \tag{5.17}$$

From statistics, sample covariance can be defined as

$$Q = \frac{1}{n}\sum_{i=1}^{n-1}(e_i - \bar{e})(e_i - \bar{e})^T \tag{5.18}$$

Standardized residuals can be obtained by dividing residuals to their standard deviations as follows:

$$\widehat{e}_i = \frac{(e_i - \bar{e})}{\sqrt{\frac{(e_i - \bar{e})^T(e_i - \bar{e})}{n-1}}} \tag{5.19}$$

Robust filtering plays an important role in orbit determination which allows measurements to be controlled and measurement noise covariance matrix to be tuned. Then, Kalman gain can be recomputed with $\bar{\mathbf{R}}_k$ as follows:

$$\mathbf{K}_{k+1} = \bar{\mathbf{P}}_{k+1}\mathbf{H}_{k+1}(\mathbf{H}_{k+1}\bar{\mathbf{P}}_{k+1}\mathbf{H}_{k+1}^T + \bar{\mathbf{R}}_k)^{-1} \tag{5.20}$$

5.4 Adaptive Kalman Filtering

Incorrect modeling of the priori noise covariance matrices of the system, $\mathbf{Q}$, can cause the filter to diverge. Since the system does not represent actual conditions in kinematic orbit determination, the noise covariance of the system needs to be well determined beforehand. An approach for optimal a priori noise covariance determination is presented in Brown and Hwang (2012). For a state consists of

PV (Position-Velocity) and clk (Clock) components, the system (process) noise covariance can be defined as follows:

$$\mathbf{Q} = \begin{bmatrix} \mathbf{Q}_{PV} & 0 & 0 & 0 \\ 0 & \mathbf{Q}_{PV} & 0 & 0 \\ 0 & 0 & \mathbf{Q}_{PV} & 0 \\ 0 & 0 & 0 & \mathbf{Q}_{clk} \end{bmatrix} \tag{5.21}$$

where $\mathbf{Q}_{PV}$ and $\mathbf{Q}_{clk}$ are expressed as:

$$\mathbf{Q}_{PV} = \begin{bmatrix} \frac{Sp\Delta t^3}{3} & \frac{Sp\Delta t^2}{2} \\ \frac{Sp\Delta t^2}{2} & \frac{Sp\Delta t^3}{3} \end{bmatrix} \quad \mathbf{Q}_{clk} = \begin{bmatrix} Sf\Delta t + \frac{Sg\Delta t^3}{3} & \frac{Sg\Delta t^2}{2} \\ \frac{Sg\Delta t^2}{2} & Sg\Delta t \end{bmatrix} \tag{5.22}$$

where Sp is the power spectral amplitude for position random process, Sf and Sg power spectral amplitudes for two white noise inputs describing clock errors for a specific clock type. While Sp can only be determined by tests on vehicle dynamics, Sf and Sg can be determined according to the Allan variances (Allan, 1966) of the clock types. In Table 5.3 various types of clocks are listed with their Allan Variance Coefficients. According to the Allan Variance coefficients, approximate power spectral amplitudes of clock errors can be calculated as:

$$S_f \sim \frac{h_0}{2} \tag{5.23}$$

$$S_g \sim 2\pi^2 h_{-2} \tag{5.24}$$

Table 5.3: Typical Allan Variance Coefficients for Common Timing Standards (Brown and Hwang, 2012)

Timing Standard	$\boldsymbol{h_0}$	$\boldsymbol{h_{-1}}$	$\boldsymbol{h_{-2}}$
TCXO[1] (low quality)	2×10^{-19}	7×10^{-21}	2×10^{-20}
TCXO (high quality)	2×10^{-21}	1×10^{-22}	2×10^{-20}
OCXO[2]	2×10^{-25}	7×10^{-25}	6×10^{-25}
Rubidium	2×10^{-22}	4.5×10^{-26}	1×10^{-30}
Cesium	2×10^{-22}	5×10^{-27}	1.5×10^{-33}

In practical applications, a priori estimation of the system noise covariance matrix may not be enough to represent the system noise of a highly dynamic system. In such systems, it is not necessary to hold system noise covariance constant. Updating system noise covariance matrix at each step allows better estimation and prevent filter divergence. In adaptive filtering, it is possible to balance dynamic model information and the measurement by tuning Kalman Gain with an adaptive factor. The adaptive gain matrix can be defined as follows:

$$\bar{\mathbf{K}}_{k+1} = \frac{1}{\alpha_k}\bar{\mathbf{P}}_{k+1}\mathbf{H}_{k+1}(\frac{1}{\alpha_k}\mathbf{H}_{k+1}\bar{\mathbf{P}}_{k+1}\mathbf{H}_{k+1}^T + \mathbf{R}_k)^{-1} \tag{5.25}$$

where α_k is the adaptive factor which can be calculated with two-segment function (Yang et al., 2001b):

$$\alpha_k = \begin{cases} 1 & |\Delta\hat{\mathbf{x}}_k| \leqslant c \\ \frac{c}{|\Delta\hat{\mathbf{x}}_k|} & |\Delta\hat{\mathbf{x}}_k| > c \end{cases} \tag{5.26}$$

where c is a threshold constant which can be chosen in the range of 1.0 to 3.0, $|\Delta\hat{\mathbf{x}}_k|$ is a learning statistic for kinematic model errors (Yang et al., 2001a). Learning statistic can be expressed with the difference between estimated and predicted state information:

$$|\Delta\hat{\mathbf{x}}_k| = \frac{\|\hat{\mathbf{x}}_k - \bar{\mathbf{x}}_k\|}{\sqrt{tr(\bar{\mathbf{P}}_{k+1})}} \tag{5.27}$$

where "tr" denotes matrix trace operation and $\bar{\mathbf{P}}_{k+1}$ is the predicted covariance matrix of the system state.

5.5 Variance Component Estimation

Since the measurement sensors from different navigation systems do not have the same quality with respect to the differences in their signal plan, noise variances and covariances of unique sensors are not expected to be equal. The variances for each observation or for particular data can be posteriorly estimated by variance component estimation based on the posteriori measurement residuals (Gao et al., 2016).

---

[1] Temperature compensated crystal oscillator

[2] Ovenized crystal oscillator

In order to estimate variance components of independent observations, various approaches are proposed in the past (Förstner, 1979; Koch, 1986; Teunissen and Amiri-Simkooei, 2008). In this thesis, the Helmert variance component estimation (HVCE) (Gopaul and Scherzinger, 2009) is adopted for the estimation of variance components of each GNSS measurement. According to the HVCE algorithm, variance factors are estimated with respect to the posteriori measurement residuals. Then a priori measurement noise covariance matrix can be calculated according to estimated variance factors. In Kalman filtering estimated residuals are calculated as follows:

$$\widehat{\mathbf{e}} = \mathbf{z} - \mathbf{H}\widehat{\mathbf{x}} \tag{5.28}$$

where $\mathbf{z}$ is the observation matrix, $\mathbf{H}$ is measurement sensitivity matrix and $\widehat{\mathbf{x}}$ is the estimated state parameter matrix. Assuming that multi-GNSS (GPS and Galileo in our case) measurements are available. Estimated residuals can be written in the matrix form as:

$$\begin{bmatrix} \widehat{\mathbf{e}}_G \\ \widehat{\mathbf{e}}_E \end{bmatrix} = \begin{bmatrix} \mathbf{z}_G \\ \mathbf{z}_E \end{bmatrix} - \begin{bmatrix} \mathbf{H}_G \\ \mathbf{H}_E \end{bmatrix} \widehat{\mathbf{x}} \tag{5.29}$$

where the subscripts *G* and *E* denotes GPS and Galileo, respectively. It should be noted that estimated residuals are calculated with the robust estimation of the state vector. Variance factor estimation (Gopaul and Scherzinger, 2009) based on HVCE theory is given as:

$$\begin{bmatrix} \sigma_G^2 \\ \sigma_E^2 \end{bmatrix} = \begin{bmatrix} s_{G,G} & s_{G,E} \\ s_{E,G} & s_{E,E} \end{bmatrix}^{-1} \begin{bmatrix} \mathbf{e}_G^T\mathbf{e}_G \\ \mathbf{e}_E^T\mathbf{e}_E \end{bmatrix} \tag{5.30}$$

where

$$s_{i,i} = n_k - 2tr(\mathbf{N}^{-1}\mathbf{N}_i) + tr(\mathbf{N}^{-1}\mathbf{N}_i\mathbf{N}^{-1}\mathbf{N}_i) \tag{5.31}$$

$$s_{i,j} = s_{j,i} = tr(\mathbf{N}^{-1}\mathbf{N}_i\mathbf{N}^{-1}\mathbf{N}_j) \tag{5.32}$$

$$\mathbf{N} = \mathbf{H}^T\mathbf{H}, \quad i,j = (G,E) \tag{5.33}$$

where n is the number of available GNSS satellites. To apply variance factors which are computed with HVCE to a robust tuned error covariance matrix, a robust scale factor is defined for each measurement. Robust weighting is kept constant during the variance component estimation process by robust scale factor:

$$\begin{bmatrix} \delta_G \\ \delta_E \end{bmatrix} = \begin{bmatrix} \bar{\mathbf{R}}_G \\ \bar{\mathbf{R}}_E \end{bmatrix} \oslash \mathbf{R}_0 \tag{5.34}$$

where "$\oslash$" stands for element-wise division operator, δ is the robust scale factor, $\bar{\mathbf{R}}$ is robust tuned variance and $\mathbf{R}_0$ is the initial measurement error variance. With respect to the calculated robust scale factors and estimated components, measurement noise covariance matrix can be redefined as follows:

$$\widehat{\mathbf{R}}_k = \begin{bmatrix} \sigma_G^2 \delta_G & 0 \\ 0 & \sigma_E^2 \delta_E \end{bmatrix} \tag{5.35}$$

For each observation group, robust estimation is performed separately to estimate measurement residuals. Robust weights are stored to calculate robust scale factor (see Eq. 5.34) for each observation. During robust estimation procedure, outliers are also detected and they are removed from observation set temporarily to not to affect estimation of variance components. As the last step before variance component estimation measurement residuals are estimated with new observation set without any outlier.

While robust weights balance the measurements in the data set, variance components weight two different data set with respect to each other. It is expected that VCE absorbs robust weights if it is applied after robust estimation procedure. However, a robust scale factor is constituted to keep robust weights constant after variance component estimation. This factor stores robust weights in the background and apply it again to the error covariances after VCE procedure. Robust Estimation and VCE integration is explained in Figure 5.3 in terms of a flowchart where all the items are related to the corresponding formulas in the chapter.

It should be noted that *removal of outliers* in Figure 5.3 is not a genuine outlier detection and removal algorithm to be applied to the observation set. It only removes outliers temporarily to estimate residuals more accurately in VCE procedure. Same outliers are later treated with robust scale factor and included in the estimated measurement noise covariance matrix.

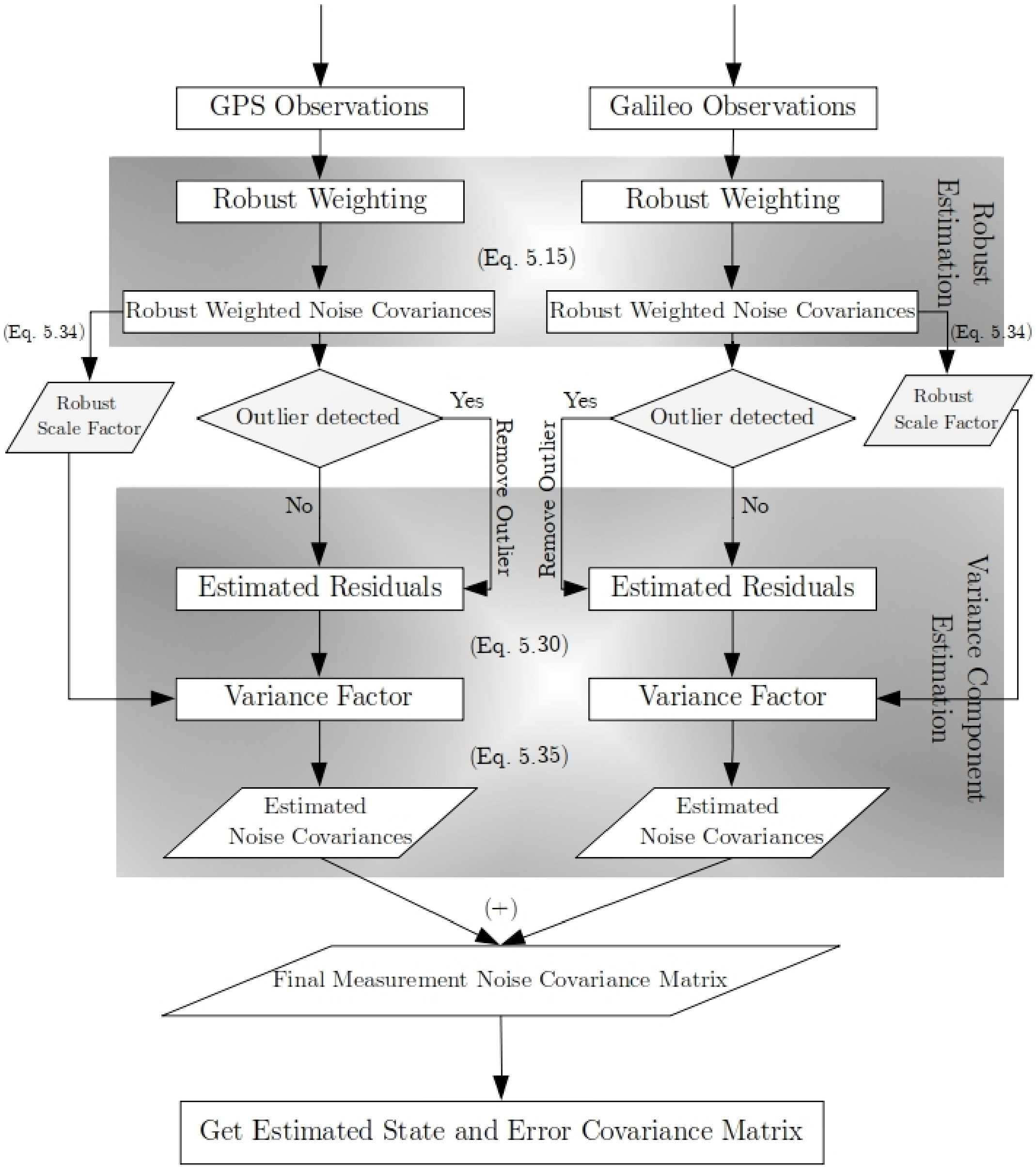

Figure 5.3: Robust Estimation and VCE Integration

CHAPTER 6

RESULTS OF ORBIT DETERMINATION AND DATA EVALUATION

In Kalman Filtering procedure, LEO GPS navigation data obtained from L1B Product of GRACE (The Gravity Recovery and Climate Experiment) mission is used for the validation of Adaptive Robust Extended Kalman filter (AREKF) approach. Data is generated by an onboard Turbo Rogue Space Receiver (TRSR) receiver which is provided by NASA's Jet Propulsion Laboratory (JPL). TRSR, also known as *BlackJack Receiver* is a modified GPS receiver which provides parallel dual-frequency code and cross-correlation tracking, and simultaneous data output from GPS satellites (Kramer, 2002). GPS broadcast ephemeris files are obtained from The Crustal Dynamics Data Information System (CDDIS) ftp server and Galileo broadcast ephemeris files and clock information for available satellite are obtained from MGEX products of International GNSS Service (IGS). All algorithms are implemented on MATLAB 2018b and developed code is run in Ubuntu 18.04 which is an open-source software operation system.

Performance of the proposed filter and the simulation is evaluated in this section.

6.1 Simulation of GPS and Galileo Orbits

Both GPS and Galileo satellite constellations are simulated according to their corresponding IGS orbit products (Hilla, 2016) or their nominal orbital parameters (European GNSS Service Centre, 2019). GPS orbits in eight orbital planes are visualized in Figure 6.1. Each orbital plane has four slots for GPS satellites. It can be seen from the figure that there are slight deviations in satellite orbits in the same orbital planes. These deviations refer to the changes in the inclination and the eccentricity values of the satellite orbit by time.

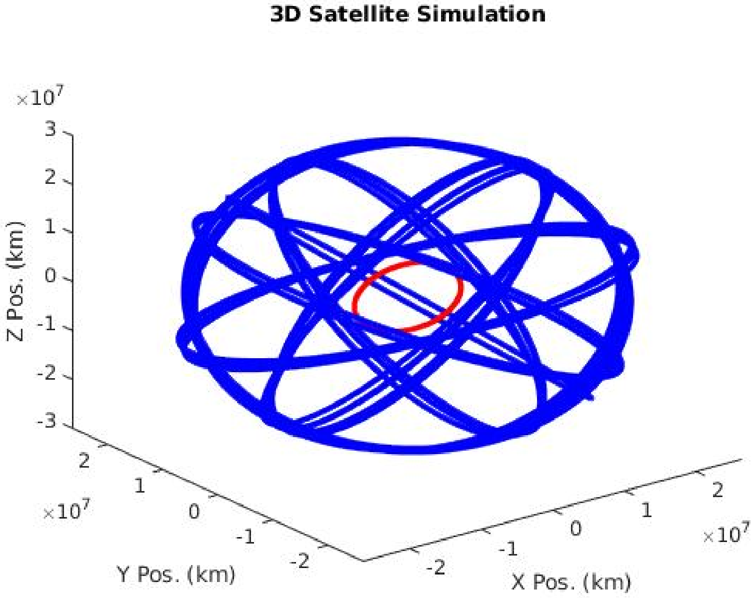

Figure 6.1: Simulated GRACE and GPS Orbits

Since Galileo orbits are simulated from the nominal orbital parameters, it is not expected to see such deviations in the orbit visualization. Eight Galileo satellites are smoothly distributed along three different orbital planes (see Figure 6.2).

Low Earth Orbit satellite GRACE is also simulated along with GNSS constellation. For the visualization, all orbits are represented in Earth Centred Inertial (ECI) frame.

6.2 Filter Settings

In Kalman Filter, some parameters need to be set initially to introduce the system attitude and measurement quality to the filter. These parameters can be set by means of measurement variance, initial error covariance matrix and system noise covariance matrix. Measurement sensor quality and the system dynamics must be known beforehand for better filter performance. In kinematic orbit determination system noise parameters should be set with larger values since the system uncertainty is assumed to be large. In order to observe general filter behavior on kinematic orbit determination Classical Extended Kalman Filter algorithm (CEKF) is tested with real

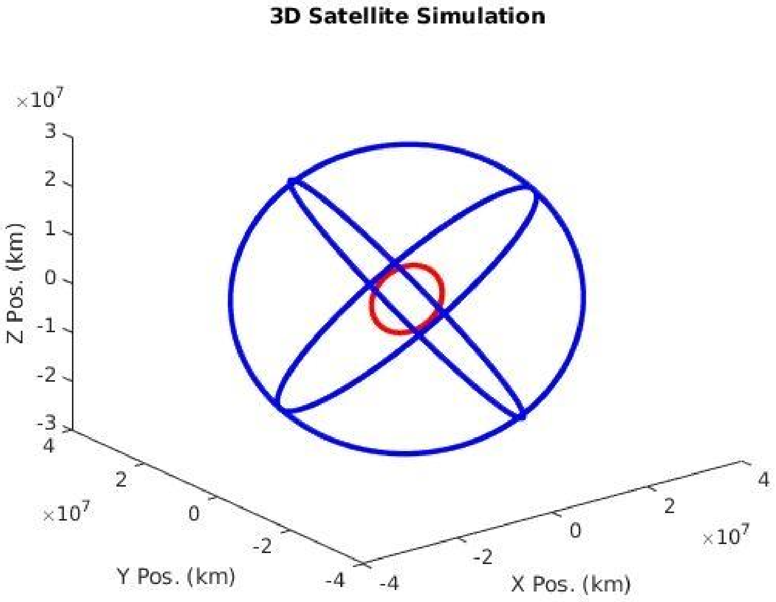

Figure 6.2: Simulated GRACE and Galileo Orbits

GRACE data as a first step. In CEKF, a simple 3σ technique is included as a default outlier detection algorithm. The technique is applied in every calculation with CEKF.

Measurement sensor noise variance is considered as 1 m. Hence, measurement error covariance matrix is given by:

$$\mathbf{R} = \begin{bmatrix} (1)^2 & 0 & 0 & 0 & 0 & 0 & 0 & 0 \\ 0 & (1)^2 & 0 & 0 & 0 & 0 & 0 & 0 \\ 0 & 0 & (1)^2 & 0 & 0 & 0 & 0 & 0 \\ 0 & 0 & 0 & (1)^2 & 0 & 0 & 0 & 0 \\ 0 & 0 & 0 & 0 & (1)^2 & 0 & 0 & 0 \\ 0 & 0 & 0 & 0 & 0 & (1)^2 & 0 & 0 \\ 0 & 0 & 0 & 0 & 0 & 0 & (1)^2 & 0 \\ 0 & 0 & 0 & 0 & 0 & 0 & 0 & (1)^2 \end{bmatrix} \tag{6.1}$$

where $R_{1,1}...R_{3,3}$ are error variance in position, $R_{4,4}...R_{6,6}$ are error variance in velocity, $R_{7,7}$ is clock bias error variance and $R_{8,8}$ is clock drift error variance. Initial state vector is estimated by kinematic positioning algorithm. Initial variances of the parameters are set as:

$$\mathbf{P}_{k_0} = \begin{bmatrix} (5)^2 & 0 & 0 & 0 & 0 & 0 & 0 & 0 \\ 0 & (5)^2 & 0 & 0 & 0 & 0 & 0 & 0 \\ 0 & 0 & (5)^2 & 0 & 0 & 0 & 0 & 0 \\ 0 & 0 & 0 & (0.05)^2 & 0 & 0 & 0 & 0 \\ 0 & 0 & 0 & 0 & (0.05)^2 & 0 & 0 & 0 \\ 0 & 0 & 0 & 0 & 0 & (0.05)^2 & 0 & 0 \\ 0 & 0 & 0 & 0 & 0 & 0 & (100)^2 & 0 \\ 0 & 0 & 0 & 0 & 0 & 0 & 0 & (1)^2 \end{bmatrix} \tag{6.2}$$

In order to determine system noise covariance matrix, power spectral amplitude for position random process S_p is substituted in the equation 5.21 and 5.22. For power spectral amplitude of 2, system noise covariance matrix is computed approximately as:

$$\mathbf{Q} = \begin{bmatrix} (25)^2 & 10 & 0 & 0 & 0 & 0 & 0 & 0 \\ 10 & (5)^2 & 0 & 0 & 0 & 0 & 0 & 0 \\ 0 & 0 & (25)^2 & 10 & 0 & 0 & 0 & 0 \\ 0 & 0 & 10 & (5)^2 & 0 & 0 & 0 & 0 \\ 0 & 0 & 0 & 0 & (25)^2 & 10 & 0 & 0 \\ 0 & 0 & 0 & 0 & 10 & (5)^2 & 0 & 0 \\ 0 & 0 & 0 & 0 & 0 & 0 & (10)^{-3} & (5.10)^{-6} \\ 0 & 0 & 0 & 0 & 0 & 0 & (5.10)^{-6} & (10)^{-6} \end{bmatrix} \tag{6.3}$$

6.3 Orbit Comparison with CEKF and AREKF using Real GPS Observation

In advance of GNSS simulation, to test the stability and robustness of proposed AREKF technique, a non-modified Extended Kalman Filter is run with specified initial settings for 5 and 24 hours of GRACE navigation data with 10 seconds of data interval. The results for each AREKF implementation are compared with real data and positions differences in each axis between estimated and true orbit are plotted with corresponding epoch number.

For real navigation data, the results of filtering procedure are interpreted with five important values; *Maximum diff. for radial* indicates the maximum radial direction difference from precise orbital positions produced by NASA's Jet Propulsion Laboratory (JPL) for 24 hours navigation data. And *RMS of differences* is the RMS value of 3D position differences from precise orbital positions by JPL along 24 hours navigation data. Rest of the results are the average differences in each component.

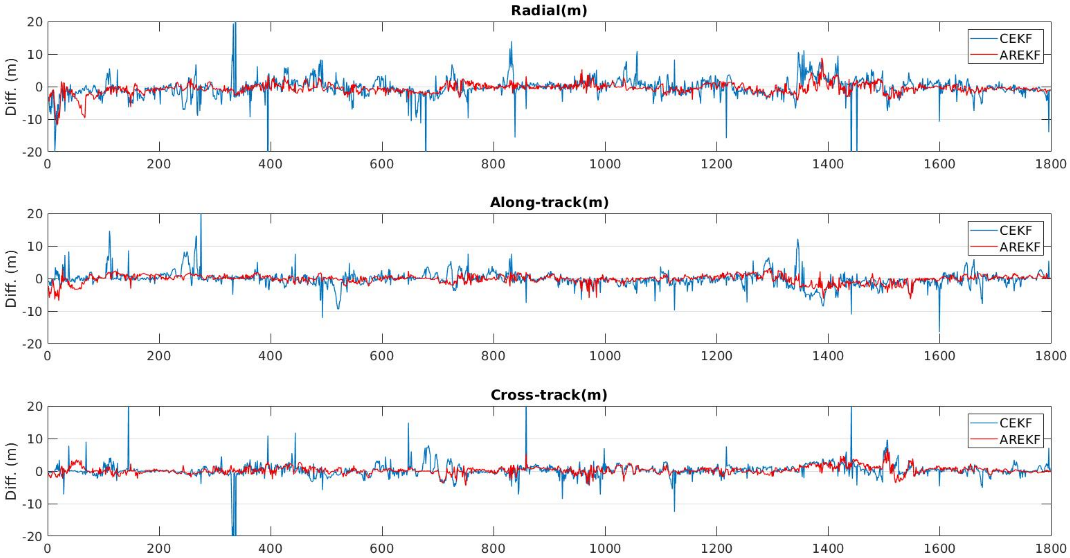

Figure 6.3: Comparison between 5 hours CEKF and AREKF RMS Results for GRACE GPS Observations from 21 Nov 2016

First, classical and improved filtering approaches are examined for 5 hours of navigation data and the results are plotted in Figure 6.3. It is seen in the figure that AREKF approach (shown in red) treated well to the measurements since the peaks in CEKF approach are disappeared in AREKF approach. As it is seen in Table 6.1, the RMS of differences between estimated and true orbit decreased from 2.25 m to 1.74 m. Maximum difference of 24 meters simply shows that classical filter's performance for kinematic orbit determination is not accurate for each epoch. And, more than 2 meters of the RMS of differences between the filter results and precise orbital positions is not accurate enough to consider CEKF process successful if the accuracy of the measurement sensor is taken into account. In order to have more information about the approach and evaluate its reliability, same procedure is applied for 24 hours navigation data (see Figure 6.4).

Table 6.1: 5-h AREKF and CEKF RMS Results for GRACE Real GPS Observations from 21 Nov 2016 ($S_p = 2$, $\sigma = 1$)

Algorithm	Max. diff. for radial (m)	3D RMS of differences (m)	Radial (m)	Along-track (m)	Cross-track (m)
CEKF	24.227	2.250	1.476	1.249	1.150
AREKF	11.594	1.738	1.207	0.932	0.834

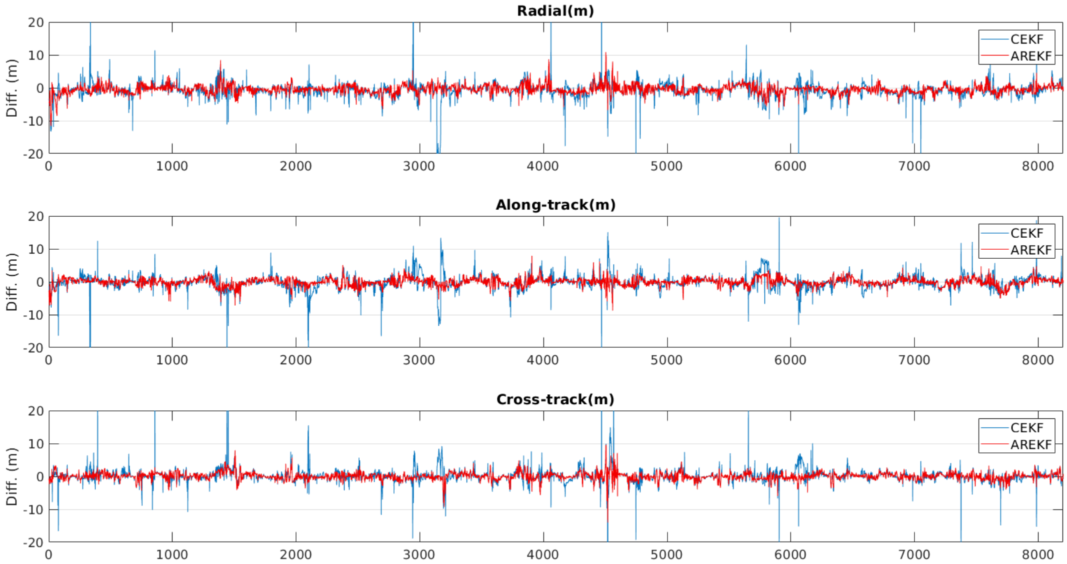

Figure 6.4: Comparison between 24 hours CEKF and AREKF RMS Results for GRACE GPS Observations from 21 Nov 2016

For both algorithms, RMS of differences from precise orbital positions are plotted in Figure 6.4. The differences in AREKF approach are significantly smaller than the classical approach. According to Table 6.2 for 24 hours of navigation data 49.2 m of maximum difference in the radial direction improved to 11.6 m and 1.6 m of RMS of differences from precise orbital positions is obtained. More than 70 cm of improvement in RMS of differences value shows that Adaptive Robust approach in Kalman filtering procedure enhancing the filter performance significantly in terms of position accuracy.

Table 6.2: 24-h AREKF and CEKF RMS Results for GRACE Real GPS Observations from 21 Nov 2016 ($S_p = 2$, $\sigma = 1$)

Algorithm	Max. diff. for radial (m)	3D RMS of differences (m)	Radial (m)	Along-track (m)	Cross-track (m)
CEKF	49.185	2.398	1.519	1.429	1.182
AREKF	11.607	1.611	1.057	0.913	0.803

6.4 Orbit Comparison with CEKF and AREKF using Simulated GPS and Galileo Observation

The filter results with simulated data are also analyzed in this section to evaluate the performance of the simulated GNSS observations and the Adaptive Robust filter approach. Simulated GNSS observations are used in the filtering procedure as input. Filtering performance on simulated navigation data is discussed. As it is stated in previous chapters, Galileo measurements are weighted differently than GPS measurements. It is expected to have better filtering performance in Galileo only orbit determination since Galileo measurements are configured to have better accuracy.

The orbit calculated with true range multilateration is taken as a reference for all comparisons and considered to be the true orbit. In Figure 6.5, the RMS values of differences between this true orbit and filter results are shown in each component for both constellations. According to the figure, Galileo-only orbit determination has a better accuracy when compared to GPS-only orbit determination. It should be noted that the measurement sensor noise values are not considered to be same since the accuracy of each constellation is different with respect to the simulated observations.

Both simulated GPS and Galileo data have outliers at three epochs. It can be seen from the figure that those outliers have no effect in the filter performance since they are weighted by robust algorithm. In Table 6.3, the accuracy of both constellations can be deduced. Since simulated data includes more consistent measurements, RMS of differences between filter results and true orbit for simulated GPS constellation are smaller than expected accuracies with predefined random measurement sensor noise values. This shows how Kalman filter deals with random noise caused by various error sources which affect the GNSS measurements. However, the improvement in

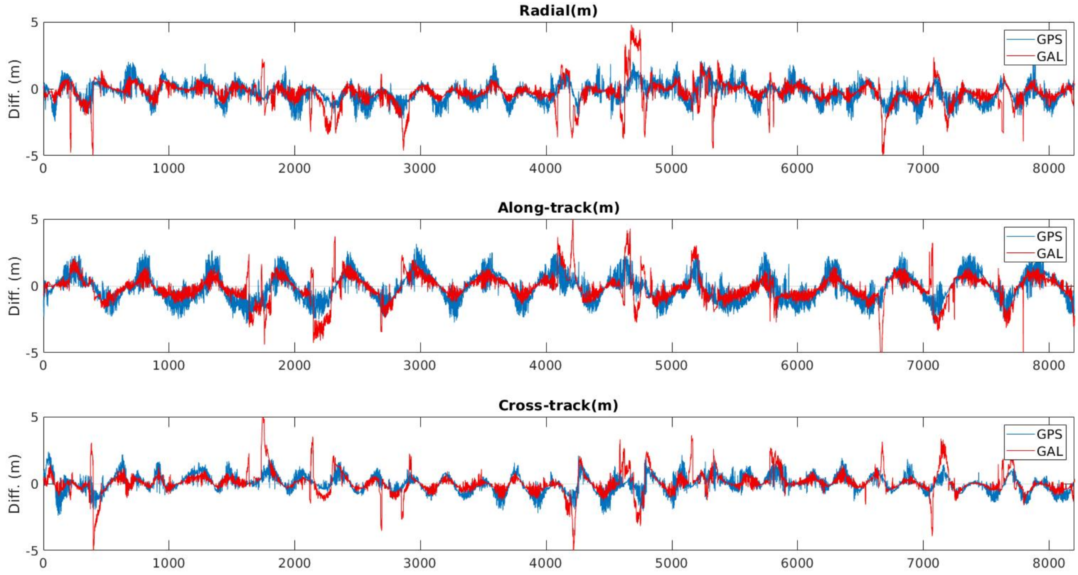

Figure 6.5: Comparison between simulated GPS and Galileo data for 21 Nov 2016

Galileo results can not be seen in the table, since the epochs with limited number of observations affected the results adversely. 5.4 m of maximum RMS difference from true orbit for radial direction can be explained with these peaks with low amount of observations.

Table 6.3: AREKF RMS Results for simulated GPS and Galileo Observations for 21 Nov 2016 ($S_p = 2$, $GPS\ \sigma = 1.36$ and $Galileo\ \sigma = 1.02$)

Constellation	Max. diff. for radial (m)	3D RMS of differences (m)	Radial (m)	Along-track (m)	Cross-track (m)
GPS	2.691	1.182	0.645	0.845	0.517
Galileo	5.412	1.127	0.635	0.764	0.531

According to results for simulated data, using only Galileo measurements is an effective way to have better orbit determination accuracy. However, the number of visible Galileo satellites for an instant is not expected to be more than the number of the satellites in GPS constellation until whole Galileo system reaches fully operational status. Therefore, Galileo observations are analyzed along with GPS measurements to evaluate the contribution of Galileo constellation.

Table 6.4 summarizes RMS values of differences from true orbit for various approaches. First, GPS-only measurements are used with 1.36 m of measurement

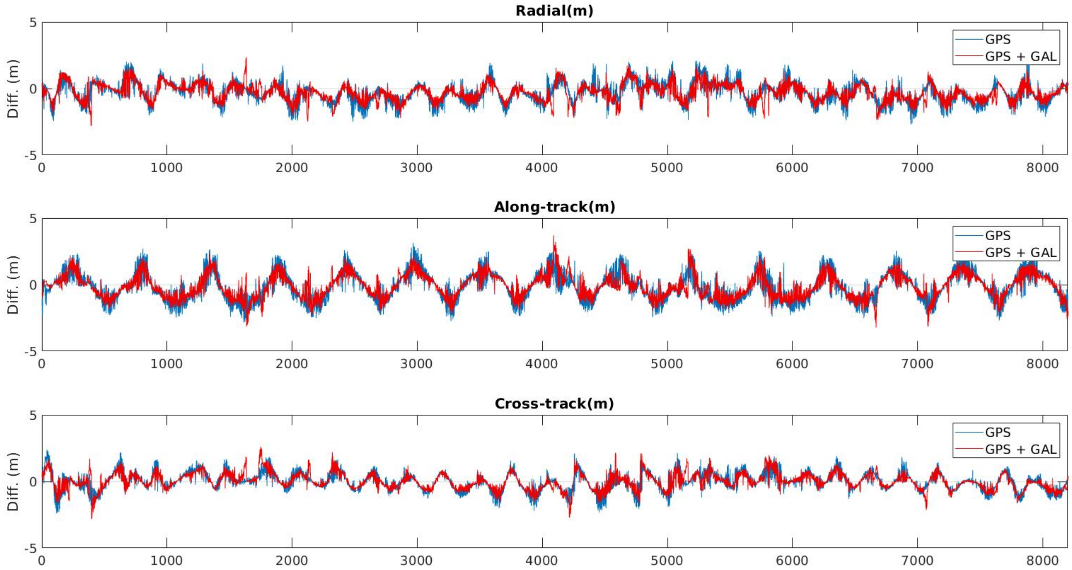

Figure 6.6: Comparison between simulated GPS-only and GPS + Galileo GRACE data for 21 Nov 2016

sensor noise in AREKF procedure. Then, GPS and Galileo measurements are combined with an equal measurement sensor value of 1 m. It can be seen from the table that, combined measurements show significantly more accurate results than GPS-only AREKF. Finally, combined measurements (also with an equal measurement sensor value of 1 m) are weighted separately in a variance component estimation (HVCE) procedure. And, the results show that the accuracy of AREKF is slightly improved to 0.98 m of RMS of differences value when HVCE procedure is implemented in the filter.

Table 6.4: RMS Results for simulated GPS-only AREKF, GPS + Galileo AREKF and GPS + Galileo AREKF with Variance Component Estimation for 21 Nov 2016 ($S_p = 2,\ \sigma = 1$ for AREKF)

	Max. diff. for radial (m)	3D RMS of differences (m)	Radial (m)	Along-track (m)	Cross-track (m)
GPS	2.691	1.182	0.645	0.845	0.517
GPS & Galileo	2.821	1.050	0.581	0.732	0.479
GPS & Galileo - HVCE	2.468	0.984	0.547	0.685	0.447

Variance component estimation is very important addition to AREKF. Using different sensors for data generation should be taken into account in terms of measurement sensor noise. Therefore, using only one noise value for measurement from both sensor affects the filter performance. According to the HVCE algorithm, variance factors are estimated with respect to the posteriori measurement residuals. Then a priori measurement noise covariance matrix can be calculated according to estimated variance factors. Kalman Filter is run with this estimated measurement noise covariance matrix and the results are compared with regular algorithm with priori defined measurement noise value.

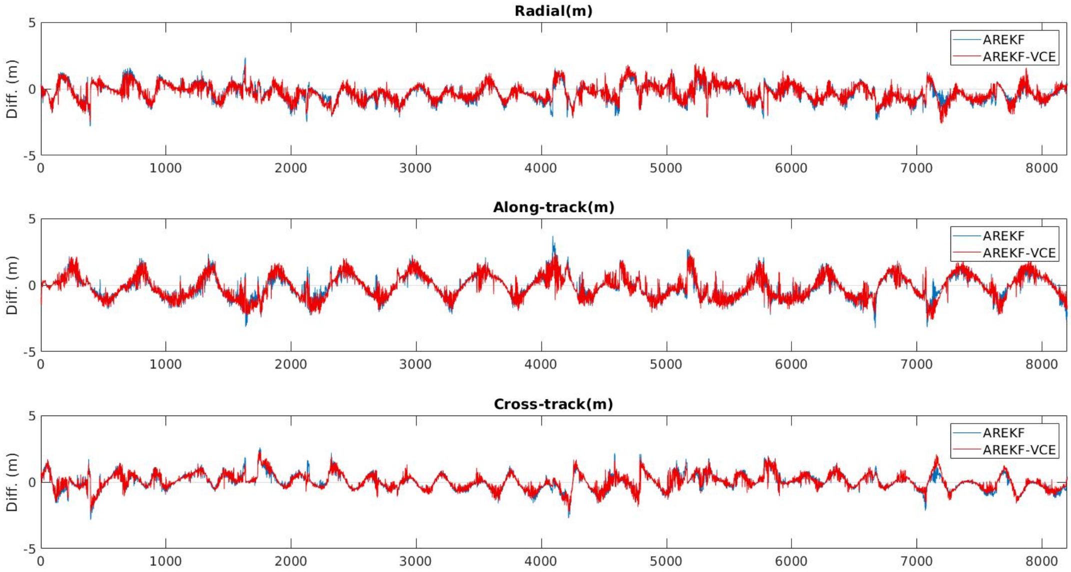

Figure 6.7: Comparison between standart AREKF and AREKF with variance component estimation for simulated GPS observations for 21 Nov 2016

CHAPTER 7

CONCLUSIONS

7.1 Summary and Conclusions

In satellite navigation, code pseudorange observations still offer accurate positioning solutions. Using dual-frequency observations and ground-based orbit determination algorithms, it is possible to obtain sub-meter level accuracy for the satellites in LEO (Montenbruck et al., 2008). As long as having sufficient number of available GNSS satellite, a robust filtering algorithm with corrected measurements can provide a solution with high level of accuracy.

In common tracking applications, there is no crucial need for detailed dynamic modeling if the measurements are reliable enough. Kinematic orbit determination has the advantage of having consistent orbit accuracy regardless of satellite altitude. Due to its affordable computational cost, kinematic orbit determination is adopted in this thesis. According to the results, 1.6 m of RMS value of the residual errors is obtained with kinematic orbit determination for 24 hours of navigation data from a LEO satellite.

A software-based GNSS constellation simulation program is developed under MATLAB 2018b environment. Whole constellation is simulated to obtain consistent data. Raw GNSS observations are generated through simulation. Both simulated and real navigation data is processed with Kalman filter and the filter performance is discussed. An extended Kalman filter is implemented with a simple dynamic system model and it performed good performance in terms on accuracy.

A robust algorithm is applied within EKF to modify measurement error covariances and regain outliers in the data set instead of getting rid of them unnecessarily. Since a simple system model is used in the prediction algorithm, system noise variances are controlled by an adaptive algorithm to prevent the filter to diverge. AREKF approach demonstrated that using these algorithms significantly increases orbit determination accuracy. In the applications which are dependent on the measurements, AREKF approach can provide accurate orbit solutions.

Additionally, Helmert Variance Component estimation is performed for weighting different sensors. A robust algorithm integrated with variance component estimation is presented as a new approach and its benefits are discussed. The results are improved 20 cm with addition of simulated Galileo observations and implementation of HVCE approach. Although the improvements in the orbital positioning accuracy are not significantly large, their effects are considerably important in space applications which require precise orbit information, such as gravity field determination, sea surface topography or high-quality radar imaging.

Simulated Galileo observations and their contribution in orbit determination are analyzed. Not only their effect in visible satellite geometry, also their low noise signal characteristics are examined. According to the simulation results, planned number of operational satellites in the Galileo constellation is not sufficient in terms of obtaining good GDOP values for GNSS receiver onboard LEO satellite. Although high quality observations are obtained from Galileo constellation, the accuracy of the orbit solution is low at some epochs due to poor satellite geometry.

7.2 Future Studies

Regarding future research about the study, some improvements and verification tests can be done in the future. Main categories of these studies can be listed as follows:

- In order to obtain more accurate state estimation, phase observations can be used in the filtering algorithm with a proper ambiguity fixing method.
- A backward smoothing algorithm can be applied to the AREKF approach for further improvements in the filter.

- When the Galileo satellites become fully operational, the algorithm can be verified with real navigation data.
- Observations from other GNSS constellations such as Glonass or BeiDou, can be analyzed with real data. When the data is fully available from all constellations, the algorithm can be applied in Real-time.

BIBLIOGRAPHY

Allan, D. W. (1966). Statistics of atomic frequency standards. *Proceedings of the IEEE*, 54(2):221–230.

Bancroft, S. (1985). An algebraic solution of the gps equations. *IEEE Transactions on Aerospace and Electronic Systems*, (1):56–59.

Basile, F., Moore, T., Hill, C., McGraw, G., and Johnson, A. (2018). Multi-frequency precise point positioning using gps and galileo data with smoothed ionospheric corrections. In *2018 IEEE/ION Position, Location and Navigation Symposium (PLANS)*, pages 1388–1398. IEEE.

Bisnath, S. B. and Langley, R. B. (2001). Precise orbit determination of low earth orbiters with gps point positioning. In *proceedings of ION National Technical Meeting*, pages 22–24.

Biswas, S., Qiao, L., and Dempster, A. (2014). Real-time on-board satellite navigation using gps and galileo measurements. In *65th International Astronautical Congress, Torronto, Canada*, pages 2–6.

Borre, K. (2009). The e1 galileo signal. *Aalborg University, Denmark.*

Bowring, B. (1985). The accuracy of geodetic latitude and height equations. *Survey Review*, 28(218):202–206.

Brown, R. G. and Hwang, P. Y. (2012). Introduction to random signals and applied kalman filtering: with matlab exercises.

Butcher, J. C. (2016). *Numerical methods for ordinary differential equations*. John Wiley & Sons.

Capuano, V., Botteron, C., and Farine, P.-A. (2013). Gnss performances for meo, geo and heo. In *Space Communications and Navigation Symposium-Space-Based Navigation Systems and Services*, number CONF.

Circiu, M.-S., Meurer, M., Felux, M., Gerbeth, D., Thölert, S., Vergara, M., Enneking, C., Sgammini, M., Pullen, S., and Antreich, F. (2017). Evaluation of gps l5 and galileo e1 and e5a performance for future multifrequency and multiconstellation gbas. *Navigation: Journal of The Institute of Navigation*, 64(1):149–163.

Eissfeller, B., Ameres, G., Kropp, V., and Sanroma, D. (2007). Performance of gps, glonass and galileo. In *Photogrammetric Week*, volume 7, pages 185–199.

Erdogan, E. (2011). *GPS-Based Real-Time Orbit Determination of Artificial Satellites Using Kalman, Particle, Unscented Kalman and H-Infinity Filters*. PhD thesis, Middle East Technical University.

European GNSS Service Centre (2019). Galileo Reference Constellation Orbital Parameters. https://www.gsc-europa.eu/system-status/orbital-and-technical-parameters. Accessed: 2019-01-09.

Fang, B. T. (1986). Trilateration and extension to global positioning system navigation. *Journal of Guidance, Control, and Dynamics*, 9(6):715–717.

Förstner, W. (1979). Ein verfahren zur schätzung von varianz-und kovarianzkomponenten. *Allgemeine Vermessungsnachrichten*, 86(11-12):446–453.

Fu, W., Huang, G., Zhang, Y., Zhang, Q., Cui, B., Ge, M., and Schuh, H. (2019). Multi-gnss combined precise point positioning using additional observations with opposite weight for real-time quality control. *Remote Sensing*, 11(3):311.

Gao, Z., Shen, W., Zhang, H., Ge, M., and Niu, X. (2016). Application of helmert variance component based adaptive kalman filter in multi-gnss ppp/ins tightly coupled integration. *Remote Sensing*, 8(7):553.

Gopaul, J.-G. W. N. and Scherzinger, B. (2009). Simplified algorithms of variance component estimation for static and kinematic gps single point positioning. *Journal of Global Positioning Systems*, 8(1):43–52.

Grewal, M. S., Andrews, A. P., and Bartone, C. G. (2013). *Global navigation satellite systems, inertial navigation, and integration*. John Wiley & Sons.

Gurtner, W. and Estey, U. (2013). The receiver independent exchange format.

Hampel, F. R., Ronchetti, E. M., Rousseeuw, P. J., and Stahel, W. A. (2011). *Robust statistics: the approach based on influence functions*, volume 196. John Wiley & Sons.

Hauschild, A., Markgraf, M., and Montenbruck, O. (2014). Gps receiver performance on board a leo satellite. *Inside GNSS*, 9(4):47–57.

Hilla, S. (2016). The extended standard product 3 orbit format (sp3-d) 21 february 2016.

Hofmann-Wellenhof, B., Lichtenegger, H., and Wasle, E. (2007). *GNSS–global navigation satellite systems: GPS, GLONASS, Galileo, and more*. Springer Science & Business Media.

Hossam-E-Haider, M., Tabassum, A., Shihab, R. H., and Hasan, C. M. (2014). Comparative analysis of gnss reliability: Gps, galileo and combined gps-galileo. In *2013 International Conference on Electrical Information and Communication Technology (EICT)*, pages 1–6. IEEE.

Huber, P. and Ronchetti, E. (1981). Robust statistics–wiley, new york. *Robust statistics. Wiley, New York.*

Jäggi, A., Beutler, G., and Hugentobler, U. (2005). Reduced-dynamic orbit determination and the use of accelerometer data. *Advances in Space Research*, 36(3):438–444.

Jazwinski, A. (1970). Stochastic processes and filtering theory. vol. 64 of math. *Science and Engineering. Academic Press. New York.*

Jäggi, A. and Arnold, D. (2017). Precise orbit determination. In Naeimi, M. and Flury, J., editors, *Global Gravity Field Modeling from Satellite-to-Satellite Tracking Data*, chapter 2, pages 35–80. Springer, Oxford.

Kaplan, E. D. and Hegarty, C. (2017). *Understanding GPS/GNSS: Principles and applications*. Artech House.

Karslioglu, M. O. (2005). An interactive program for gps-based dynamic orbit determination of small satellites. *Computers & geosciences*, 31(3):309–317.

Karslioglu, M. O., Erdogan, E., and Pamuk, O. (2017). Gps-based real-time orbit determination of low earth orbit satellites using robust unscented kalman filter. *Journal of Aerospace Engineering*, 30(6):04017063.

Keil, E. M. (2014). *Kalman Filter Implementation to Determine Orbit and Attitude of a Satellite in a Molniya Orbit*. PhD thesis, Virginia Tech.

Klobuchar, J. A. (1987). Ionospheric time-delay algorithm for single-frequency gps users. *IEEE Transactions on aerospace and electronic systems*, (3):325–331.

Koch, K. (1986). Maximum likelihood estimate of variance components. *Bulletin Gæodésique*, 60(4):329–338.

Kramer, H. J. (2002). *Observation of the Earth and its Environment: Survey of Missions and Sensors*. Springer Science & Business Media.

Langley, R. B. (1997). Gps receiver system noise. *GPS world*, 8(6):40–45.

Li, K., Zhou, X., Guo, N., Zhao, G., Xu, K., and Lei, W. (2017a). Comparison of precise orbit determination methods of zero-difference kinematic, dynamic and reduced-dynamic of grace-a satellite using shorde software. *Journal of Applied Geodesy*, 11(3):157–165.

Li, M., Xu, B., and Zhang, L. (2017b). Orbit determination for remote-sensing satellites using only optical imagery. *International journal of remote sensing*, 38(5):1350–1364.

Montenbruck, O. (1992). Numerical integration methods for orbital motion. *Celestial Mechanics and Dynamical Astronomy*, 53(1):59–69.

Montenbruck, O. and Gill, E. (2012). *Satellite orbits: models, methods and applications*. Springer Science & Business Media.

Montenbruck, O., Issler, J., Markgraf, M., Mercier, F., Santandrea, S., Garcia, A., Naudet, J., and Serre, S. (2010). Gps based precise orbit determination and real-time navigation of the proba-2 spacecraft. In *5th ESA Workshop on Satellite Navigation Technologies*.

Montenbruck, O., Markgraf, M., Garcia-Fernandez, M., and Helm, A. (2008). Gps for microsatellites–status and perspectives. In *Small Satellites for Earth Observation*, pages 165–174. Springer.

Montenbruck, O., Van Helleputte, T., Kroes, R., and Gill, E. (2005). Reduced dynamic orbit determination using gps code and carrier measurements. *Aerospace Science and Technology*, 9(3):261–271.

Pany, T., Eissfeller, B., and Winkel, J. (2003). Tracking of high bandwidth gps/galileo signals with a low sample rate software receiver. In *Proc. GNSS*. Citeseer.

Pascual, D., Park, H., Camps, A., Alonso, A., and Onrubia, R. (2013). Comparison of gps l1 and galileo e1 signals for gnss-r ocean altimetry. In *2013 IEEE International Geoscience and Remote Sensing Symposium-IGARSS*, pages 358–361. IEEE.

Peng, D. and Wu, B. (2009). Precise orbit determination for jason-1 satellite using on-board gps data with cm-level accuracy. *Chinese Science Bulletin*, 54(2):196–202.

Peyret, F., Gillieron, P. Y., Ruotsalainen, L., and Engdahl, J. (2015). Sappart white paper: Better use of global navigation satellite systems for safer and greener transport.

Psiaki, M. L., Huang, L., and Fox, S. M. (1993). Ground tests of magnetometer-based autonomous navigation (magnav) for low-earth-orbiting spacecraft. *Journal of Guidance, Control, and Dynamics*, 16(1):206–214.

Sarnadas, R. and Ferreira, T. (2011). Nusar-a software platform to process gps/galileo os signals. *Journal of Aerospace Engineering*, 3(1):92.

Seeber, G. (2003). Satellite geodesy, 2nd completely revised and extended edition. *Walter de Gruyter GmbH & Co. KG*, 10785:303–304.

Sirola, N. (2010). Closed-form algorithms in mobile positioning: Myths and misconceptions. In *2010 7th Workshop on Positioning, Navigation and Communication*, pages 38–44. IEEE.

Sleewaegen, J.-M., De Wilde, W., and Hollreiser, M. (2004). Galileo altboc receiver. In *Proceedings of GNSS*, pages 16–19.

Subirana, J. S. S., Zornoza, J. J., and Hernández-Pajares, M. (2011). Ionosphere-free combination for dual frequency receivers. https://gssc.esa.int/navipedia/index.php/Ionosphere-free_Combination_for_Dual_Frequency_Receivers. Accessed: 2019-04-18.

Švehla, D. and Rothacher, M. (2002). Kinematic orbit determination of leos based on zero or double-difference algorithms using simulated and real sst gps data. In *Vistas for geodesy in the new millennium*, pages 322–328. Springer.

Swatschina, P. (2009). Dynamic and reduced-dynamic precise orbit determination of satellites in low earth orbits.

Tavella, P. (2008). Statistical and mathematical tools for atomic clocks. *Metrologia*, 45(6):S183–S192.

Teunissen, P. J. and Amiri-Simkooei, A. (2008). Least-squares variance component estimation. *Journal of geodesy*, 82(2):65–82.

Tukaram, A. S. (2014). Development of orbit determination system software for low earth orbit leo satellite using global positioning system gps data for on board use.

Vallado, D. A. (2001). *Fundamentals of astrodynamics and applications*, volume 12. Springer Science & Business Media.

Vetter, J. R. (2007). Fifty years of orbit determination. *Johns Hopkins APL technical digest*, 27(3):239.

Viswanathan, M. (2013). Simulation of digital communication systems using matlab. *Mathuranathan Viswanathan at Smashwords*.

Wu, S.-C., Yunck, T. P., and Thornton, C. L. (1991). Reduced-dynamic technique for precise orbit determination of low earth satellites. *Journal of Guidance, Control, and Dynamics*, 14(1):24–30.

Yang, Y. (2010). Adaptively robust kalman filters with applications in navigation. In *Sciences of Geodesy-I*, pages 49–82. Springer.

Yang, Y., He, H., and Xu, G. (2001a). Adaptively robust filtering for kinematic geodetic positioning. *Journal of geodesy*, 75(2-3):109–116.

Yang, Y., Song, L., and Xu, T. (2002). Robust estimator for correlated observations based on bifactor equivalent weights. *Journal of Geodesy*, 76(6-7):353–358.

Yang, Y.-x., Xu, T.-h., and He, H. (2001b). On adaptively kinematic filtering. *Selected Papers for English of Acta Geodetica et Cartographica Sinica*, 200(1):25–32.

Yeganehsahab, A. (2016). Estimation of ionospheric threat model parameters for gbas using gnss data for marmara region. Master's thesis, Retrieved from METU Library (http://etd.lib.metu.edu) .

Yeh, T.-K., Hwang, C., Xu, G., Wang, C.-S., and Lee, C.-C. (2009). Determination of global positioning system (gps) receiver clock errors: impact on positioning accuracy. *Measurement Science and Technology*, 20(7):075105.

Yoon, Y. T., Eineder, M., Yague-Martinez, N., and Montenbruck, O. (2009). Terrasar-x precise trajectory estimation and quality assessment. *IEEE Transactions on Geoscience and Remote Sensing*, 47(6):1859–1868.

Yunck, T. P., Melbourne, W. G., and Thoenton, C. (1985). Gps-based satellite tracking system for precise positioning. *IEEE transactions on geoscience and remote sensing*, (4):450–457.

Zappulla, R. and Spencer, D. (2013). Prox-1 guidance, navigation & control formulation and algorithms. *Georgia Institute of Technology*.

Appendix A

APPENDIX

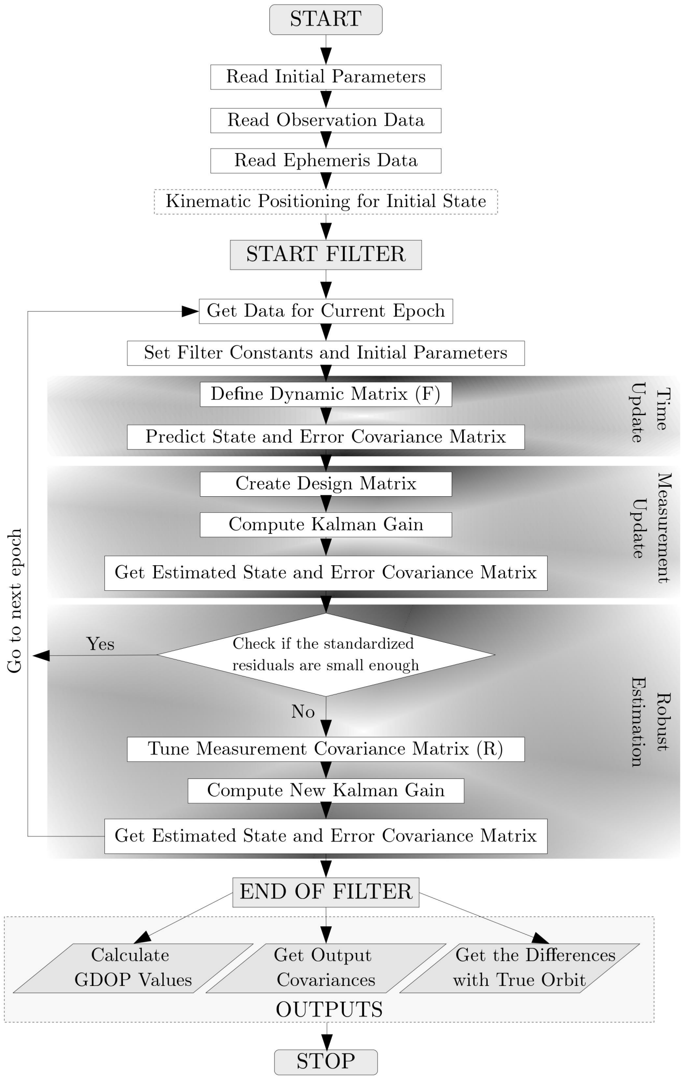

Figure A.1: Adaptive Robust Extended Kalman Filter Flowchart

Appendix B

APPENDIX

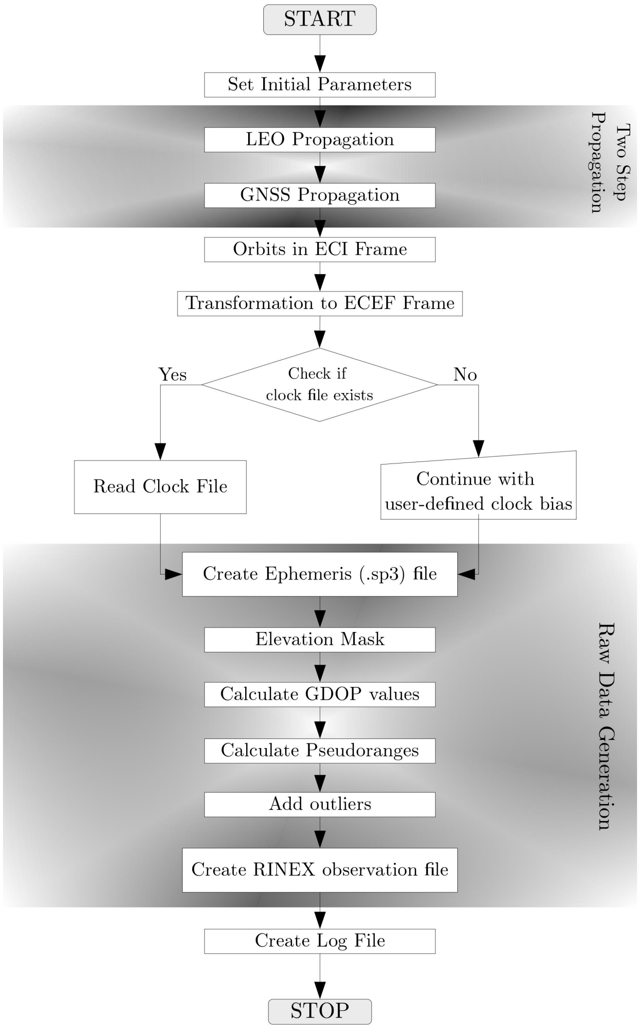

Figure B.1: GNSS Orbit Simulation Flowchart